Indian Journal of Biochemistry & Biophysics
Vol. 62, August 2025, pp. 827-853
DOI: 10.56042/ijbb.v62i8.16568

In silico exploration of selected coumarin derivatives as potential antioxidant: Insights from DFT, NBO, Hirshfeld surface, ADMET profiling, Molecular docking and Dynamics simulations

Rituraj Barman[1], Benzir Ahmed[1], Hemchandra Deka[2], Pratyashee Barukial[1], Debabrat Baishya[2] & Bipul Bezbaruah[1]*

[1]Department of Applied Sciences; & [2]Department of Bioengineering and Technology, Gauhati University, Guwahati-781 014, Assam, India

Received 22 January 2025; revised 07 March 2025

Coumarin derivatives have been explored as highly promising antioxidants due to their significant binding mechanisms with radicals and protein residues. Herein, we have selected a few bioactive coumarin derivatives to investigate their effectiveness in complexation with alkoxy ($RO^{\bullet}$) and hydroperoxyl ($HOO^{\bullet}$) radicals as well as with carbonic anhydrase VII (CA VII) protein. To gain further insights, *in silico* studies *viz*., DFT, pharmacokinetic evaluation (ADMET) and drug-likeness assessments, *etc*., are useful to analyze the complex formation mechanism with radicals and protein residues. Again, Molecular Electrostatic Potential (MEP), Spin Density (SD) and Natural Bond Orbital (NBO) studies display superior binding interactions with the protein residues characterized by conventional H-bonding along with other hydrophobic interactions. Moreover, molecular docking, dynamics and physicochemical analysis reveal that all coumarin derivatives interact effectively within the internal cavity of CA VII, detailing binding affinities and specific protein residues involved.

Keywords: ADMET, CA VII, Coumarin derivatives, Molecular docking, Molecular dynamics

Reactive oxygen species (ROS) include entities such as superoxide ($O_2^{\bullet-}$), hydroperoxyl ($HOO^{\bullet}$), hydroxyl ($OH^{\bullet}$), alkoxy ($RO^{\bullet}$) *etc*., radicals are a group of molecules generated from oxygen, which are extremely reactive due to the presence of unpaired electrons[1]. However, excessive ROS generation disrupts cellular redox equilibrium, interacting with organic molecules and triggering a chain reaction of oxidative damage. This can further harm proteins, lipids and DNA, potentially leading to the cause of various disorders[2]. Antioxidants inhibit oxidative reactions by neutralizing free radicals, thereby reducing cell damage and helping to prevent associated illnesses. Naturally occurring antioxidants originate from various sources, including vitamin C and E, zinc, selenium, flavonoids, polyphenols, carotenoids and spices like ginger and turmeric[3]. One of the best-known phenolic compounds showing notable antioxidant activities is naturally occurring coumarin and some of its derivatives *viz*., esculetin, scopoletin and umbelliferone stand out for various health benefits. These compounds have extensively been researched due to its wide range of pharmacological properties such as antibacterial, anti-inflammatory and antioxidant qualities. Chicory and horse chestnut plants contain esculletin whereas scopoletin is found in black mulberry and noni fruit. Similarly, umbelliferone is present in a wide variety of vegetables, such as coriander and carrots[4].

The cytosolic enzyme known as carbonic anhydrase VII (CA VII) is associated with the human brain plays a crucial role in normal *in vivo* mechanisms, like reversible hydration of CO_2. Recent investigations on the metabolic processes of the enzyme reveal that coumarin derivatives are recognized as potential inhibitors and therapeutic antioxidants, as they favorably interact with CA VII, contributing to the regulation of oxidative stress in brain tissues[5]. This interaction supports the development of new CA VII inhibitors for treating neurological disorders linked to oxidative damage. By reducing ROS generation, these inhibitors help mitigate oxidative stress[6].

Herein, we have selected some of the naturally occurring coumarin derivatives *viz*., α-pyrone ring

*Correspondence:
Phone: +91-9854634789 (Mob)
E-mail: bipulbezbaruah@gmail.com
Suppl. Data available on respective page of NOPR

based chromen-2-one (C1), 6,7-dihydroxychromen-2-one (C2), 7-hydroxy-6-methoxychromen-2-one (C3) and 7-hydroxychromen-2-one (C4); which are considered as active antioxidant agents[7].

Leveraging their structural compatibility, we computationally explore the impact of free radicals (RO$^{\bullet}$ and HOO$^{\bullet}$) on these coumarin derivatives and their non-covalent interactions with CA VII. Furthermore, using DFT method, we have analyzed HOMO-LUMO, NBO, MEP and Spin Density distributions to assess possible changes in their electronic structures. Moreover, Hirshfeld surface and molecular visualization analysis *viz*., NCI, VMD and ELF will also be carried out for the antioxidant-radical complexes; identifying possible interacting sites, changes in molecular conformation and electron density. Again, molecular docking is also considered as a very convenient tool for investigating the most favoured interacting sites between antioxidants and protein residues. Further, ADMET profile analysis, drug-likeness evaluation, molecular dynamics simulations and other physicochemical studies provide deeper insights into their antioxidant potential.

Computational methodology

We have introduced Density functional theory (DFT) tool to analyze the non-covalent interactions existing between selected coumarin derivatives as antioxidant agents and free radicals (RO$^{\bullet}$and HOO$^{\bullet}$). All the molecular structures were initially constructed using GaussView5.0 and then optimization was initiated at the M06-2X functional level with 6-311G++(d,p) basis set using Gaussian09 software packages[8]. In addition, joinMolecule and Arguslab software packages were used to generate and visualize all the constructed models[9]. The interaction energy of the coumarin derivatives and RO$^{\bullet}$/HOO$^{\bullet}$ radical complexes can be calculated using the following equation:

$$\text{Interaction Energy (IE)} = E_{A\text{-}R} - E_A - E_R \quad \ldots(1)$$

where; $E_{A\text{-}R}$, E_A and E_R are the respective single point energies of the antioxidant-radical complex, antioxidants and radicals.

Significant quantum chemical calculations were also conducted to analyze different physicochemical properties, for the radical complexes. Additionally, the study included molecular docking to investigate the potential interaction between antioxidant agents and protein residue (CA VII). Again, the minimal binding affinities and ligand efficacies of small molecules against target substrates were determined using the SeamDock online application[10]. Further, we employed ADMET (Absorption, Distribution, Metabolism, Excretion and Toxicity) analysis, a crucial aspect of drug discovery tool, to assess the physicochemical characteristics, drug-likeness and pharmacokinetic parameters of the coumarin derivatives[11].

Results and Discussion

Interaction of RO$^{\bullet}$ and HOO$^{\bullet}$ radicals with coumarin derivatives

In this investigation, certain coumarin derivatives were primarily selected based on their compatible molecular structure; specifically, the presence of at least one phenolic hydroxyl group, excluding the parent coumarin molecule, as displayed in (Fig. 1 and Table 1). This structural feature of coumarin derivative enhances the reactivity towards RO$^{\bullet}$ and HOO$^{\bullet}$ radicals. Our comprehensive quantum chemical analysis of the coumarin derivatives and radical species revealed highly favorable binding affinities, as evidenced by the computed interaction energy (IE) values as depicted in (Table 2). In theoretical calculations, it is evident that more negative IE values usually indicate greater stability in molecular complexes[12]. The observed trend in computed IE value suggests that coumarin derivatives may exhibit potential antioxidant properties, attributed to their ability to effectively scavenge RO$^{\bullet}$ and HOO$^{\bullet}$ radicals. Based on their computed IE calculations, the sequence of stability of the coumarin derivatives and RO$^{\bullet}$/HOO$^{\bullet}$ radical complexes are found as follows:

For RO$^{\bullet}$ radical complexes:C2 < C3 < C1 < C4

For HOO$^{\bullet}$ radical complexes:C2 < C3 < C1 < C4

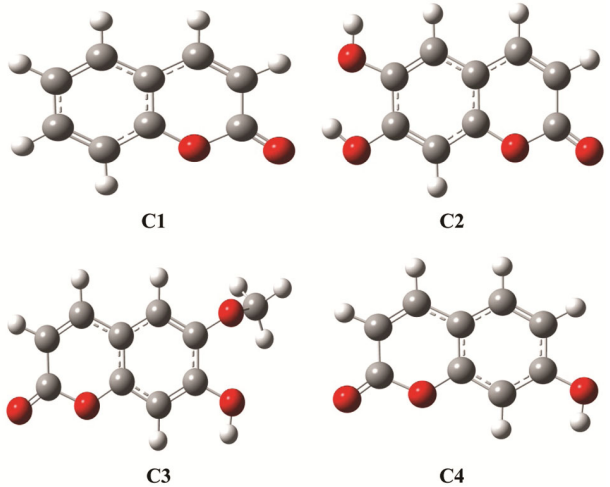

Fig. 1 — Optimized structures of Antioxidants C1, C2, C3 and C4

Table 1 — IUPAC and common name of some Coumarin derivatives as antioxidant agents

Coumarin Derivatives	IUPAC Name	Common Name
C1	chromen-2-one	Coumarin
C2	6,7-dihydroxychromen-2-one	Esculetin
C3	7-hydroxy-6-methoxychromen-2-one	Scopoletin
C4	7-hydroxychromen-2-one	Umbelliferone

Table 2 — Minimized stacked Interaction energy (kcal/mol) for Coumarin derivatives with RO•/HOO•radicals

Coumarin derivatives	Interaction Energies (kcal/mol)	
	RO•	HOO•
C1	-3.08	-3.79
C2	-0.51	-0.82
C3	-2.44	-3.13
C4	-3.31	-4.26

The observed stability trend among the coumarin derivatives highlights that the antioxidant C4 *i.e.*, umbelliferone exhibits significantly higher binding affinity towards RO• and HOO• radicals. This is evidenced by its higher negative IE values of -3.31 and -4.26 kcal/mol for C4 with RO• and HOO• radical complexes, respectively, as shown in (Table 2); which indicates that it could be attributed to effective non-covalent interactions within the adduct. On the other hand, C1 consistently shows lower negative IE values, closely trailing the stability of the C4-RO•/HOO• radical complex. Notably, the C2, esculetin, exhibits the least negative IE values of -0.51 kcal/mol and -0.82 kcal/mol, indicating less favourable binding with RO• and HOO• radicals compared to the other derivatives *i.e.*, C2 has the least scavenging power towards the radicals.

The interaction within the C4-RO•/HOO• radical complexes are efficiently analyzed due to the presence of an active phenolic -OH group. The molecular structure of C1 and C4, featuring a benzene ring fused to an α-pyrone ring, facilitates smooth interactions with RO• and HOO• radicals (Fig. 2). Additionally, the α-pyrone ring plays a dual role in maintaining charge neutrality and facilitating H-bond donation. As a result, the C4-radical complex exhibits stronger interactions than other coumarin derivatives, further enhanced by the formation of a remote H-bond at C4 with the radicals. However, the presence of two -OH groups in C2, influences the stability of the C2-RO•/HOO• radical complex; but, the steric hindrance around the reactive site may reduce accessibility to the radicals, resulting in lower IE value with a less stable radical complex (Fig. 2). Consequently, C2 exhibits a weaker binding affinity for RO• and HOO• radicals compared to the other studied antioxidants.

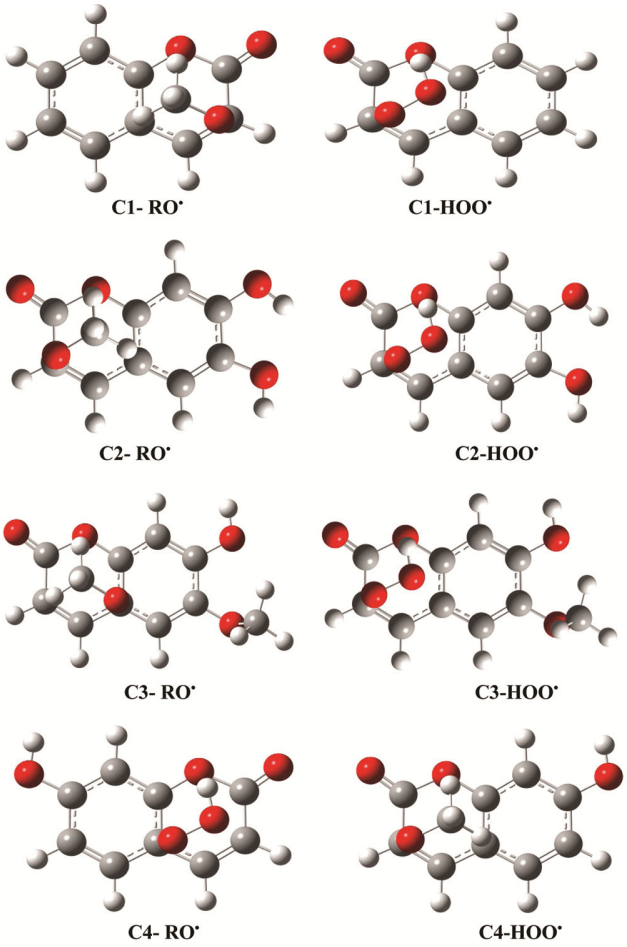

Fig. 2 — Minimized models for Antioxidants (C1, C2, C3 and C4) with RO• and HOO• radical complexes

Specificity in the radical-antioxidant interactions

The HOO• radical complexes result in more negative IE values than that of RO• radical complexes; indicating stronger binding affinity with HOO• than that of RO• radicals (Table 2). Hence, the selected antioxidants may be recognized as truly HOO•radical specific. For example, in C4-radical complexes the IE values of HOO•and RO• complexes are found to be -4.26 and -3.31 kcal/mol, respectively, exhibits a higher specificity to HOO• radicals. Moreover, the less favorable C2-radical complex shows the least preferred binding towards HOO•with a lower IE value of -0.82 kcal/mol. A detailed comparison of the IE and binding affinities of these antioxidant-radical complexes are shown in (Table 3).

Theoretical Insights into antioxidant mechanism

The interaction mechanism between antioxidants and free radicals exhibits a notable ability to neutralize free radicals through various mechanisms. Among all the studied antioxidants, C4 exhibited the

Table 3 — Probable interacting sites of the Coumarin derivatives and their binding specificity towards RO•/HOO• radicals

Coumarin derivatives	Preferred radicals	Radical specificity	Favoured interacting sites	Unfavoured interacting sites
C1	RO•/HOO•	HOO•	α-pyrone ring	Benzene ring
C2	RO•/HOO•	HOO•	α-pyrone ring	Benzene ring
C3	RO•/HOO•	HOO•	α-pyrone ring	Benzene ring
C4	RO•/HOO•	HOO•	α-pyrone ring	Benzene ring

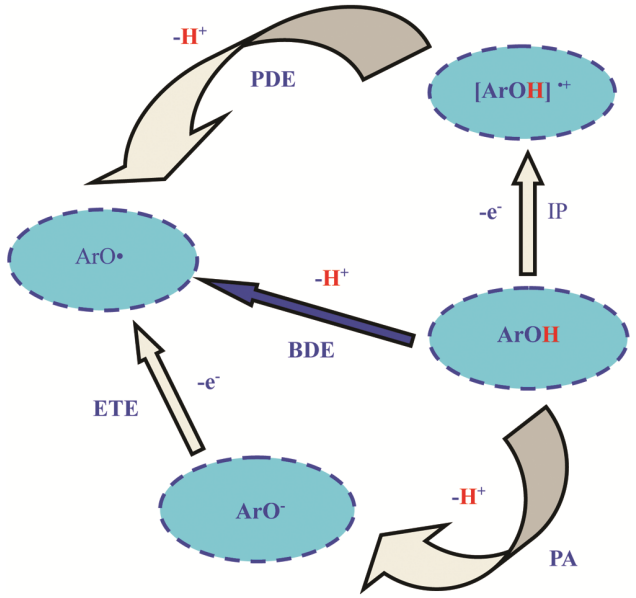

Fig. 3 — Schematic diagram of Antioxidant mechanisms

highest antioxidant activity, due to its more negative IE values as calculated for C4-radical complexes; consequently, C4 was chosen for further investigation. The primary pathways involve Hydrogen Atom Transfer (HAT), Sequential Proton Loss Electron Transfer (SPLET) and Single-Electron Transfer coupled with Proton Transfer (SET-PT)[13]. A schematic diagram for these theoretical mechanisms is shown in (Fig. 3). Each of these pathways offers a distinct strategy through which coumarin-based substances alleviate oxidative stress by efficiently donating or transferring protons and electrons. This action stabilizes reactive free radicals, thereby preventing potential cellular damage[14].

a) Hydrogen Atom Transfer (HAT) mechanism

The HAT mechanism is a common pathway through which antioxidants exhibit their protective effects against oxidative stress. Herein, an antioxidant donates a H-atom to a free radical, neutralizing it and stabilizing itself in the process. This reaction is characterized by the cleavage of the bond holding the H-atom to the antioxidant, leading to the formation of a new radical derived from the antioxidant and a neutral molecule.

The HAT mechanism can be represented by the following reaction:

$$ArOH + X^{\bullet} \rightarrow ArO^{\bullet} + XH \quad \ldots(2)$$

This reaction is most dominant when the dissociation energy of the O-H bond is minimal, allowing antioxidant (ArOH) to effectively trap the free radical. This highlights the significance of calculating the bond dissociation energy (BDE) to determine the stability of ArOH and its subsequent reactivity with the free radical. The most effective antioxidants are those with the lowest BDE, as they demonstrate a higher rate of free radical inhibition[15].

The BDE for the HAT mechanism can be calculated as follows:

$$BDE = H(ArO^{\bullet}) + H(H^{\bullet}) - H(ArOH) \quad \ldots(3)$$

The calculated BDEs for O-H bonds of C4 in RO• and HOO• radical complexes are found to be 108.12 and 102.43 kcal/mol respectively, shown in (Table 4). As C4-HOO• complex exhibits lower BDE, hence it becomes more readily neutralized. The lower BDE also corresponds to a weakened O-H bond of C4, which facilitates the antioxidant's ability to donate a H-atom more effectively; thereby enhancing its scavenging efficiency against the radicals. The electron-deficient nature of the HOO• radical further destabilizes the O-H bond of C4, promoting easier dissociation. Conversely, RO• is less reactive than HOO• radicals, as it requires higher energy to break the O-H bond, as indicated by the higher BDE values. This suggests a moderate antioxidant activity of C4 w. r. t. RO•; where H donation is relatively less feasible as compared to HOO• radical complexes. The electron-withdrawing nature of RO• and HOO• radicals significantly impact the bond strength. But, the strong electron-withdrawing effect of HOO• radical weakens the O-H bond of C4 the most; thereby enhancing its antioxidant's ability to donate H. Therefore, our calculations indicate that the sequence of BDEs as shown in (Table 4), directly correlates with the antioxidant potential towards RO• and HOO• radicals.

b) Sequential Proton Loss Electron Transfer (SPLET)

The SPLET mechanism consists of two primary steps as shown below:

Table 4 — Bond dissociation enthalpy (BDE), ionization potential (IP), Proton dissociation enthalpy (PDE), Proton affinity (PA) and Electron transfer enthalpy (ETE) of antioxidant C4 with RO$^{\bullet}$ and HOO$^{\bullet}$ radicals in gas phase

Antioxidants	Positions	HAT	SPLET		SET-PT	
		BDE	PA	ETE	IP	PDE
C4	-OH	108.12	212.64	56.76	186.90	152.08
		102.43	248.09	42.65	153.06	144.54

Step 1. Firstly, the antioxidant (ArOH) releases a proton, producing an anion (ArO^-):

$$ArOH \rightarrow ArO^- + H^+ \quad \ldots(4)$$

This reaction is influenced by the calculated proton affinity (PA) values which can be calculated as:

$$PA = H(ArO^-) + H(H^+) - H(ArOH) \ldots\ldots\ldots (5)$$

Step 2. Secondly, the free radical ($X^{\bullet}$) captures the electron from by the anion (ArO^-), leading to the formation of the stable radical ($ArO^{\bullet}$):

$$ArO^- + H^+ + X^{\bullet} \rightarrow ArO^{\bullet} + XH \quad \ldots(6)$$

In this chemical reaction, the electron transfer enthalpy (ETE) serves as the key thermodynamic parameter which is calculated by the following equation:

$$ETE = H(ArO^{\bullet}) + H(e^-) - H(ArO^-) \quad \ldots(7)$$

In SPLET mechanism, the antioxidant activity of C4 with RO$^{\bullet}$ and HOO$^{\bullet}$ radicals depend on the calculated PA and ETE values. The -OH group in C4's structure may influence these values, affecting the antioxidant activity by modulating the electronic environment around the O-H bond of C4[16]. For the C4-HOO$^{\bullet}$ radical complex with computed PA and ETE values are found to be 248.09 and 42.65 kcal/mol; the higher PA facilitates easier proton loss and the lower ETE value indicates efficient electron transfer, resulting in high antioxidant activity. Again, in C4-RO$^{\bullet}$ radical complex PA and ETE value are found to be 212.64 and 56.76 kcal/mol, leading to a moderate antioxidant activity due to more challenging proton dissociation and electron transfer reaction.

c) Single-electron transfer followed by proton transfer (SET-PT)

This mechanism also follows a two-step reaction process:

Step 1. During the initial step, the antioxidant transfers an electron to the free radical ($X^{\bullet}$), forming a radical cation ($ArOH^{\bullet+}$):

$$ArOH + X^{\bullet} \rightarrow ArOH^{\bullet+} + X^- \quad \ldots(8)$$

The numerical parameter that defines this mechanism is the ionization potential (IP):

$$IP = H(ArOH^{\bullet+}) + H(e^-) - H(ArOH) \quad \ldots(9)$$

Step 2. This step involves the decomposition of the cationic antioxidant into a stable radical.

$$ArOH^{\bullet+} \rightarrow ArO^{\bullet} + H^+ \quad \ldots(10)$$

This mechanism evaluates antioxidant efficiency based on the proton dissociation enthalpy (PDE):

$$PDE = H(ArO^{\bullet}) + H(H^+) - H(ArOH^{\bullet+}) \quad \ldots(11)$$

In SET-PT mechanism, the efficiency of the first step depends on the IP of the antioxidant, which represents the energy required to remove an electron; whereas the second step is influenced by the PDE, representing the energy required to remove a H^+ from the radical cation[17].The computed IP and PDE values for C4-radical complexes indicate a greater favorability for interaction with HOO$^{\bullet}$ rather than RO$^{\bullet}$ radical; as C4-HOO$^{\bullet}$ radical complex results in lower IP and PDE values of 153.06 and 144.54 kcal/mol in comparison to C4-RO$^{\bullet}$ radical complex *i.e.*, 186.90 and 152.08 kcal/mol as shown in (Table 4). Hence, SET-PT mechanism highlights the most effective antioxidant property for C4 towards any ROS; particularly for HOO$^{\bullet}$ radical, due to its efficient electron transfer property followed by proton loss steps. However, the optimal mechanism also depends on the specific radical and the structural characteristics of the antioxidants.

Electronic property analysis

a) Molecular Electrostatic Potential (MEP)

The MEP is a well-recognized parameter for the visual comprehension of physicochemical features *viz*., electron density, relative polarity, electrophilic/nucleophilic sites, electrostatic potential regions *etc*., which are typically analyzed by observing the colour changes occur across the surface of a molecule[18]. Herein, an electron-rich (negative) region, being the preferred site for an electrophilic attack is represented by the red-coloured surface; whereas electron deficient (positive) blue-coloured region indicating nucleophilic site and electrostatically neutral region is represented by green coloured surface as illustrated in (Fig. 4). The colour scale in MEP changes from deepest red to blue, in case of C1, the MEP ranges from -0.085 to +0.085 a.u., while for C2, the range is broader, spanning from -0.130 to +0.130 a.u.

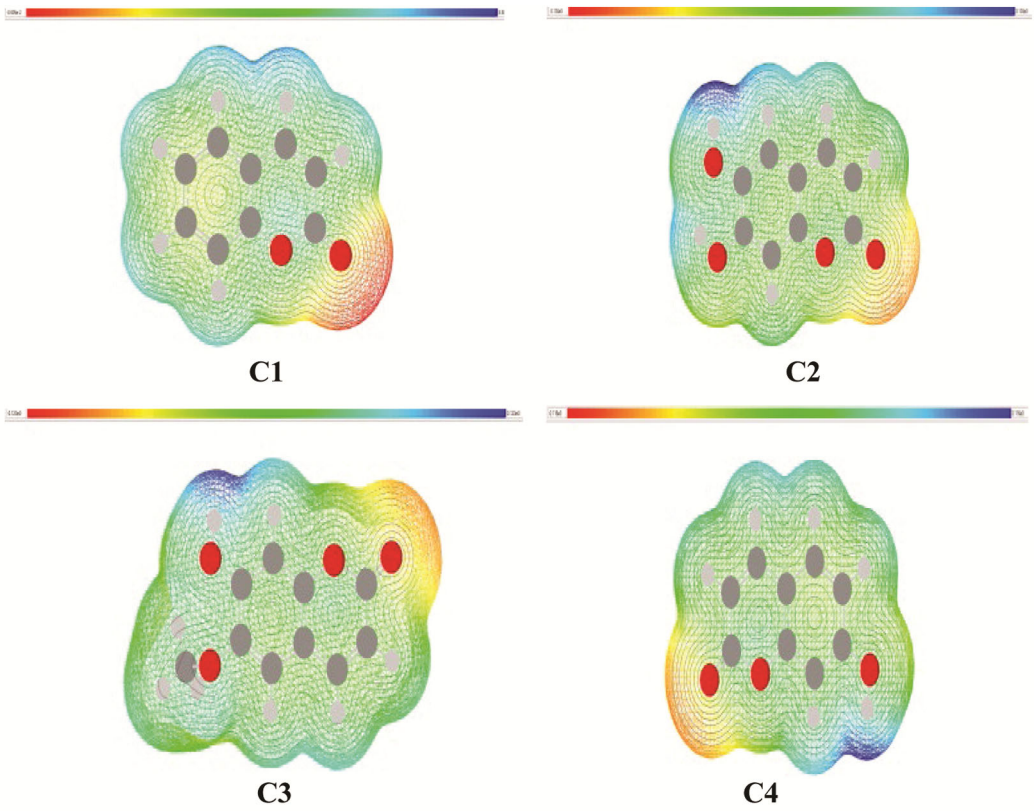

Fig. 4 — Molecular electrostatic potential (MEP) maps of C1, C2, C3 and C4

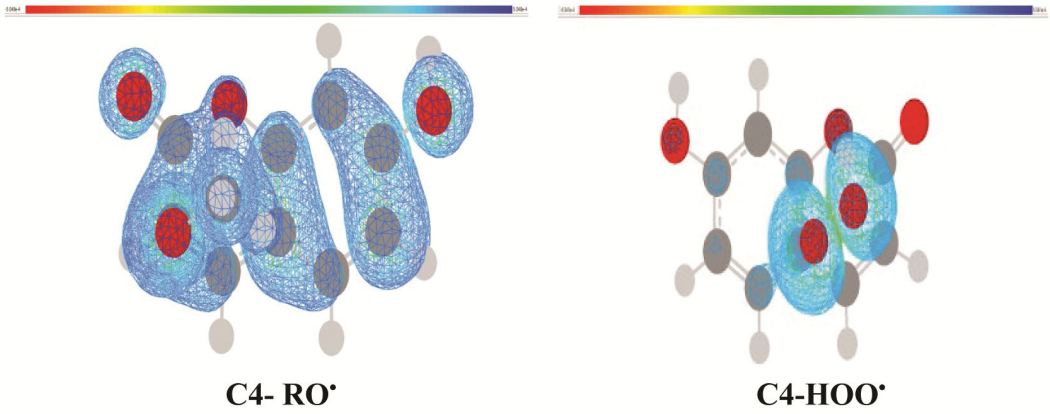

Fig. 5 — Spin density (SD) distribution map for C4-RO•/HOO•complexes

In the case of C3, the potential range is slightly narrower, extending from -0.123 to +0.123 a.u. and for C4, the MEP values lie between -0.116 and +0.116 a.u., respectively. It has been observed that all studied coumarin derivatives possess an active electronegative region which will be the probable interacting sites for free radical interaction (Fig. 4).

b) Spin density (SD) distribution

Computed SD is a crucial quantum chemical parameter for evaluating the radical scavenging potential of antioxidants[19]. The spin density distribution of antioxidant-radical complexes has been analyzed, with blue regions in the distribution map indicating positive isovalues across the radical complexes. As antioxidants donate an electron to a reactive free radical, the antioxidant itself transforms into a new radical. The stability of this resultant radical is largely determined by the electron spin density distribution within its structure, as shown in (Fig. 5 and Suppl. Fig. 1). Greater spin density delocalization enhances radical stability, thereby

improving its efficiency in neutralizing free radicals. Specifically, the spin density of the C4-HOO• radical complex is notably higher as compared to other three complexes, indicating greater stabilization of the HOO• radical within the complex.

c) Natural bond orbital (NBO) analysis

NBO analysis provides valuable insights into electron charge distribution mechanism, bond polarization and delocalization within a molecular system; which is very effective for detailed understanding of intra/inter molecular charge transfer, resonance structure, bonding characteristics and the stability of a chemical entity[20]. In our case, as the antioxidant C4 results in effective interaction with HOO•and RO• radicals, hence NBO was computed only for C4 and its radical complexes. Thus, the NBO analysis of C4 reveals effective π*-π* interaction between $\pi^*C_5–C_6 \rightarrow \pi^*C_1–C_2$ and $\pi^*C_3–C_4 \rightarrow \pi^*C_{12}–C_{13}$ bonds, with stabilizing interaction energy (E^2) of 253.43 and 85.15 kcal/mol, respectively, which highlights the significant role of the π-electrons in stabilizing C4 molecule (Table 5A). Additionally, the lone pair (LP) interaction, $LP_2O_{16} \rightarrow \sigma^*C_{14}–O_{15}$ also contributes to the molecule's stabilization, albeit to a lesser extent *i.e.*, 45.19 kcal/mol, as shown in (Table 5A). Again, in C4-RO• radical complex, the π*-π* interaction becomes weakened, as the E^2 values for $\pi^*C_5– C_6 \rightarrow \pi^*C_1 – C_2$ interactions decreases to 128.42 kcal/mol. These reduced E^2 value of C4-RO•radical complex indicates that the RO• radical disrupts the stabilizing electronic interaction within C4; although, the π*-π* delocalization remains the dominant contributor, as shown in (Table 5B). Again, introduction of HOO• radical to C4 alters the possible π*-π* electron interaction in the radical complex. But interestingly, in C4-HOO• radical complex, the favorable π*-π* interactions are $\pi^*C_5–C_6 \rightarrow \pi^*C_1 – C_2$ and $\pi^*C_3–C_4 \rightarrow \pi^*C_1–C_{22}$ with E^2 values 104 and 112.95 kcal/mol, respectively (Table 5B). This shift suggests that HOO• radical initiates new pathways for electron delocalization, modifying the electronic structure of the molecule. However, in both the radical complexes $LP_2\ O_{16}\rightarrow\sigma^*C_{14}–O_{15}$ transition occurs with minimum changes in E^2 values which is relatively insignificant as compared to the π*-π* interactions. Hence, the NBO analysis clearly reveals that RO• and HOO• significantly alter the π*-π* electron delocalization within the C4 molecule in their radical complexes, providing insight into the changes in antioxidant behavior in response to these reactive species.

d) Mulliken charge (MC) distribution analysis

The objective of MC distribution analysis is to explore how the electronic properties of these compounds influence their antioxidant activity. This is essential in reducing the oxidative stress and protecting the biological systems from damage induced by free radicals[21]. We could determine the influence of RO• and HOO• radicals on any antioxidants by examining the possible changes occur in MC distribution at the reactive sites within the antioxidant-radical complexes. It has observed that in antioxidants C1 and C4, the α-pyrone ring predominantly interacts with RO• and HOO• radicals, whereas, in C2 and C3, -OH and -OCH_3 groups are responsible for this interaction. The potential

Table 5A — The computed NBO analysis for the most prominent antioxidant (C4) and RO•/HOO• radicals highlight key interactions and their E^2 energies

Compounds	Donor NBO (i) → Acceptor NBO (j)	E^2 kcal/mol	E(j)-E(i) a.u.	F(i,j) a.u.
C4	$\pi^*C_5 – C_6 \rightarrow \pi^*C_1 – C_2$	253.43	0.01	0.094
	$\pi^*C_3 – C_4 \rightarrow \pi^*C_{12} – C_{13}$	85.15	0.03	0.082
	$LP_2\ O_{16} \rightarrow \sigma^*C_{14} – O_{15}$	45.19	0.71	0.162
RO•	$LP_3\ O_5 \rightarrow \sigma^*\ C_1\text{-}H_2$	6.13	0.68	0.082
	$LP_2\ O_5 \rightarrow \sigma^*\ C_1\text{-}H_3$	3.70	0.72	0.066
HOO•	$LP_3O_3 \rightarrow \sigma^*\ O_1\text{-}H_2$	2.33	0.69	0.051
	$\sigma\ O_1\text{-}H_2 \rightarrow \sigma^*\ O_1\text{-}O_3$	1.16	0.68	0.032

Table 5B — The Computed NBO analysis for the most prominent antioxidant (C4) with RO• and HOO• radical complexes with E^2 energies

Compounds	Donor NBO (i) → Acceptor NBO (j)	E^2 kcal/mol	E(j)-E(i) a.u.	F(i,j) a.u.
C4- RO•	$\pi^*C_5 – C_6 \rightarrow \pi^*C_1 – C_2$	128.42	0.02	0.094
	$\pi^*C_3 – C_4 \rightarrow \pi^*C_{12} – C_{13}$	124.42	0.02	0.094
	$LP_2\ O_{16} \rightarrow \sigma^*C_{14} – O_{15}$	22.7	0.71	0.162
C4- HOO•	$\pi^*C_3 – C_4 \rightarrow \pi^*C_1 – C_{22}$	112.95	0.02	0.094
	$\pi^*C_5 – C_6 \rightarrow \pi^*C_1 – C_2$	104.00	0.02	0.094
	$LP_2\ O_{16} \rightarrow \sigma^*C_{14} – O_{15}$	22.72	0.71	0.162

interaction occurs through one C and two O atoms of the said interacting ring, as slight changes observed in their MC distribution. The MC distribution analysis of the interacting C and O atoms for individual antioxidants and radical complexes shown in (Table 6A), which reveals notable variations in the charge density among the antioxidants. Similarly, the MC density of the O atoms in RO$^{\bullet}$ and HOO$^{\bullet}$ radicals also vary before and after interaction with the antioxidants, as depicted in (Table 6B). Hence, on introducing RO$^{\bullet}$ and HOO$^{\bullet}$ radicals significantly alter the charge distribution on C and O atoms of the antioxidants, affecting their reactivity and stability.

HOMO-LUMO and Physicochemical property analysis

The highest occupied (HOMO) and lowest unoccupied (LUMO) molecular orbitals collectively known as frontier molecular orbitals (FMOs), provide key information about the molecular behavior. A molecule's propensity to transfer electrons is reflected in the HOMO, which is correlated to its antioxidant and nucleophilic characteristics. On the other hand, the LUMO, which usually refers electrophilic behavior, describes a molecule's ability to accept electrons. Usually, wider HOMO-LUMO energy gap (ΔE_{gap}) shows greater molecular stability, lower reactivity and decreased sensitivity to charge transfer[22]. Moreover, chemical potential, hardness, softness and electrophilicity index are just a few of the chemical reactivity descriptors, which may be computed using following equations:

$$\text{Chemical Potential, } (\mu) = \tfrac{1}{2}\,(E_{LUMO} + E_{HOMO}) \quad \ldots(12)$$

$$\text{Chemical Hardness, } (\eta) = \tfrac{1}{2}\,(E_{LUMO} - E_{HOMO}) \quad \ldots(13)$$

$$\text{Chemical Softness, } (S) = 1/\eta \quad \ldots(14)$$

$$\text{Electrophilicity index, } (\omega) = \mu^2/2\eta \quad \ldots(15)$$

Generally, harder chemical complexes with larger ΔE_{gap} values are associated with greater stability; while smaller ΔE_{gap} values indicate softer molecules with increased reactivity. The electron transfer process is typically evaluated based on the chemical potential (μ). A more negative μ value indicates a strong electron-donating ability of a system, while a less negative μ value suggests a tendency toward electron-accepting behaviour[23].

We observed notable differences in the physicochemical parameters of the coumarin derivatives as shown in (Table 7A-C) and (Fig. 6 and Suppl. Fig. 2). Antioxidant, C4 is categorized as a softer molecule due to its exceptionally lower ΔE_{gap} value of 0.5034 eV as compared to the other compounds; while C1 with significantly higher ΔE_{gap} value *i.e.* 3.4052 eV, indicating that it is harder in nature. These differences show that in comparison to other coumarin derivatives, C4 has higher kinetic instability which enhances its chemical reactivity. Again, the electron donor-acceptor behavior *i.e.*, the chemical potential (μ) value of C4 exhibits higher negative value of -13.6347 eV, which shows its significant electron-donating ability; whereas, C2 shows the lowest negative value of -10.0209 eV, indicating its potential electron accepting ability. In addition, C4 has a lower chemical hardness (η) value *i.e.* 0.2517 eV and high chemical softness (S) value of 3.9729 eV^{-1} indicating more reactive agent in contrast to other antioxidants. Again, for C4-HOO$^{\bullet}$ radical complex shows a higher η value of 0.5032 eV than

Table 6A — Computed Mulliken Charge distribution of some selected Antioxidants with individual compound and RO$^{\bullet}$ and HOO$^{\bullet}$ radicals

Antioxidants/Radical Complexes	Interacting sites	Mulliken Charges		
		C	O	O
C1		0.182	-0.071	-0.291
C1-RO$^{\bullet}$	α-pyrone ring	-0.014	-0.085	-0.251
C1-HOO$^{\bullet}$		-0.042	-0.111	-0.265
C2		0.197	-0.081	-0.292
C2-RO$^{\bullet}$	α-pyrone ring	-0.152	-0.127	-0.253
C2-HOO$^{\bullet}$		-0.035	-0.121	-0.266
C3		0.189	-0.082	-0.289
C3-RO$^{\bullet}$	α-pyrone ring	-0.017	-0.137	-0.257
C3-HOO$^{\bullet}$		-0.035	-0.125	-0.263
C4		0.183	-0.081	-0.290
C4-RO$^{\bullet}$	α-pyrone ring	0.003	-0.099	-0.248
C4-HOO$^{\bullet}$		-0.030	-0.108	-0.259

Table 6B — Computed Mulliken Charge distribution of selected RO$^{\bullet}$ and HOO$^{\bullet}$ radicals

Selected Radicals	Interacting sites	Mulliken Charges	
		O_a	O_b
RO$^{\bullet}$		-0.143	----
C1-RO$^{\bullet}$	α-pyrone ring	-0.062	----
HOO$^{\bullet}$		-0.135	-0.142
C1-HOO$^{\bullet}$		-0.130	-0.063
RO$^{\bullet}$		-0.143	----
C2-RO$^{\bullet}$	α-pyrone ring	-0.051	----
HOO$^{\bullet}$		-0.135	-0.142
C2-HOO$^{\bullet}$		-0.131	-0.066
RO$^{\bullet}$		-0.143	----
C3-RO$^{\bullet}$	α-pyrone ring	-0.070	----
HOO$^{\bullet}$		-0.135	-0.142
C3-HOO$^{\bullet}$		-0.127	-0.067
RO$^{\bullet}$		-0.143	----
C4-RO$^{\bullet}$	α-pyrone ring	-0.061	----
HOO$^{\bullet}$		-0.135	-0.142
C4-HOO$^{\bullet}$		-0.122	-0.085

*O_a- $HO_aO^{\bullet}$/$RO^{\bullet}_a$ and O_b- $HOO^{\bullet}_b$

Table 7A — Energies E_{LUMO}, E_{HOMO} and E_{gap} for the studied individual Coumarin derivatives

Compounds	E_{LUMO} (ev)	E_{HOMO} (ev)	E_{gap} (ev)
C1	-6.0202	-9.4254	3.4052
C2	-5.7331	-8.5756	2.8424
C3	-5.7576	-8.8009	3.0433
C4	-8.9220	-9.4254	0.5034

Table 7B — Computed Chemical reactivity parameters for the individual Coumarin derivatives

Compounds	Chemical Potential (μ)	Chemical Hardness (η)	Softness (s)	Electrophilicity index (ω)
C1	-10.7329	1.7026	0.5873	98.0674
C2	-10.0209	1.4212	0.7036	10.0209
C3	-10.1581	1.5216	0.6571	10.1581
C4	-13.6347	0.2517	3.9729	13.6347

Table 7C — Computed Chemical reactivity parameters for minimized adducts of Coumarin derivatives with the most preferred HOO• radical

Compounds	Chemical Potential (μ)	Chemical Hardness (η)	Softness (s)	Electrophilicity index (ω)
C1- HOO•	-9.6538	0.1190	8.4021	12.3762
C2- HOO•	-8.7988	0.4113	2.4309	38.0962
C3- HOO•	-9.0256	0.3032	3.2919	29.0473
C4- HOO•	-9.8503	0.5032	1.9872	24.4123

the individual C4 *i.e.*, 0.2517, suggesting that C4-HOO• complex attains a more stable conformation. Similarly, for C4-HOO• complex shows lower S value of 1.9872 eV^{-1} than that of individual C4 *i.e.* 3.9729 eV^{-1}, enhancing the stability of C4-HOO• radical complex. As a result, C4 is none the less soft and possibly more reactive than its radical complex. Again, the computed μ value for C4-HOO•complex is found to be -9.8503 eV, which indicates considerable electron-accepting activity; but, the individual C4 retains its electron-donating properties with high μ value of -13.6347 eV. The electrophilic nature of the C4-HOO• complex is further supported by its high electrophilicity index (ω) value *i.e.* 24.4123 eV, as depicted in (Table 7B-C). Hence, the HOMO-LUMO analysis reveals that C4-HOO• radical complex reflects higher chemical stability with electrophilic nature, which significantly enhances its antioxidant potential.

The Hirshfeld surface analysis

Hirshfeld surface (HS) analysis typically reveals electron density contributions and intermolecular forces essential for crystal packing stability. Herein, Crystal Explorer version 21.5 was employed to study the crystal structure of the antioxidants, focusing on

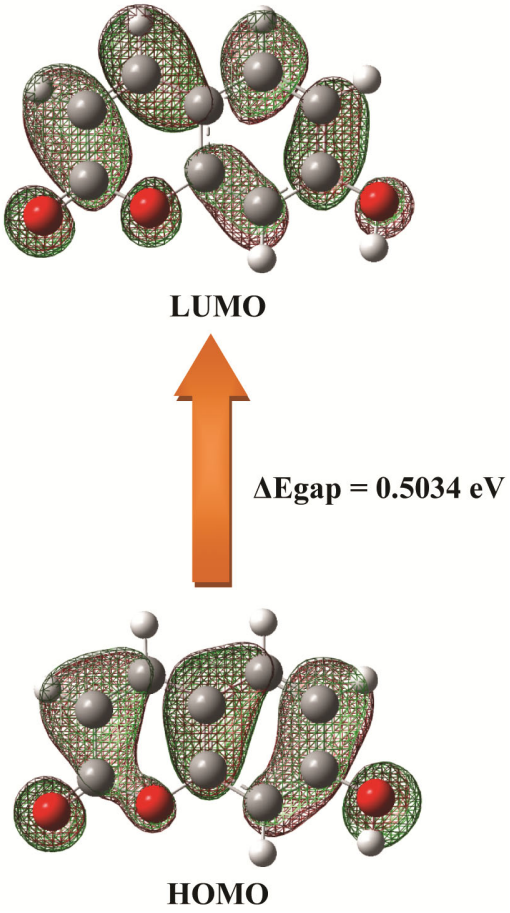

Fig. 6 — HOMO-LUMO plots of the Antioxidant, C4

intermolecular interactions that influence its properties. The parameters d_i (distance from the surface to the nearest internal atom) and d_e (distance to the closest external atom) were essential for precisely characterizing the interaction environment. The resulting 2D fingerprint plots, which display the distribution and density of surface points, were colour-coded based on contact density. This provides an intuitive visualization of significant non-covalent interactions, including hydrogen bonding, van der Waals (vdW) forces and π-π stacking interaction[24].

The HS analysis highlighted key intermolecular interactions within the crystal structure of the most favored antioxidant, C4. The d_{norm} mapping, spanning a range from -0.700 to 1.367, revealing the notable features. In particular, prominent deep red spots signifies strong hydrogen bonding involving the O-atom of the -OH group and O-atoms within the antioxidant system as shown in (Fig. 7A). The bonding characteristics observed in the crystal structure are further verified by normalized distance

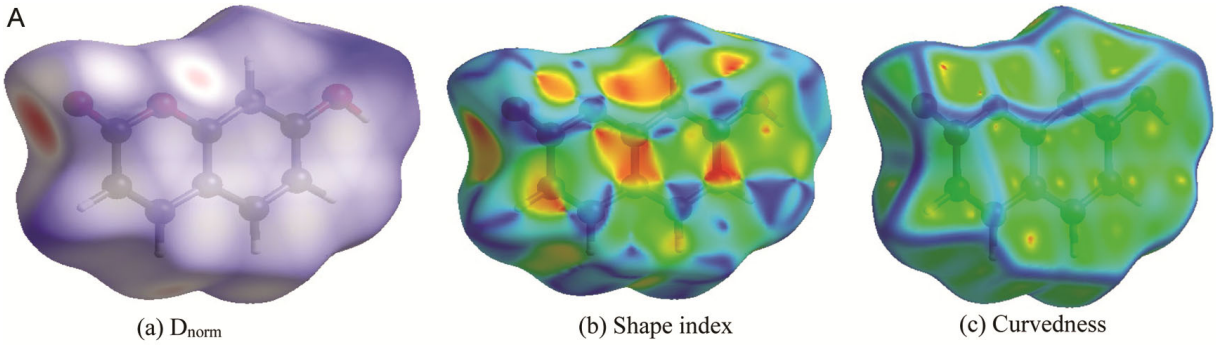

Fig. 7A — Hirshfeld surface mapped with (a) $d_{norm,}$ (b) shape-index and (c) curvedness of Antioxidant, C4

mapping, which employs a colour-coded scheme to highlight key aspects of the crystal's packing arrangement[25]. Blue areas indicate long contacts, red areas signify short contacts and white areas represent distances equal to the sum of the vdW radii. This analysis visually depicted the spatial arrangement of molecules within the crystal lattice. The shape index mapping (ranging from -1.0 to +1.0) and curvedness mapping (ranging from -4.0 to +4.0) were used to describe the surface properties. The curvedness map revealed an absence of flat surface regions, indicating almost negligible π-π interactions (Fig. 7A). Notably, the 2D-fingerprint plot features a pair of distinct spikes in the lower left region, indicating short d_i and d_e values as shown in (Fig. 7B). This suggests that antioxidant C4 acts as both H-acceptor (represented by the lower spike, where $d_i > d_e$) and H-donor (shown by the upper spike, where $d_i < d_e$). The colour scheme uses yellow, green and purple to represent high, medium and low-density points in the corresponding regions, respectively.

A comprehensive analysis of all intermolecular interactions, combined with detailed fingerprint plots showing individual contributions, provided an in-depth understanding of the interaction landscape. For antioxidant C4, the percentage contributions of different intermolecular contacts were determined, indicating significant interactions such as H···H (27.2%), O···H (22.8%)/H···O (18.6%), C···C (11.2%) and C···H (8.9%)/H···C (5.2%) respectively as displayed in (Fig. 7B). These results underscore the critical role of H-bonding and other contacts in defining the crystal structure of C4, which influence its interacting properties.

NCI, RDG, VMD and ELF Analysis

Non-covalent interaction (NCI) and reduced density gradient (RDG) analysis are considered as very effective tools for understanding intermolecular interactions within molecular complexes. This technique allows for the identification and characterization of specific interacting regions, which is essential for determining the nature and strength of both weak and strong directional forces. NCI analysis identifies regions in molecular systems where non-covalent interactions occur, including vdW forces, hydrogen bonding and steric hindrances. By analyzing electron density (ρ) and its derivatives, it provides detailed insights into the spatial distribution and properties of these interactions[26]. The RDG is a function used to highlight regions of low electron density with non-covalent interactions, as defined by:

$$RDG = \frac{I\nabla\rho I}{2(3\pi^2)^{1/3}\rho^{4/3}}$$

Where, ∇ρ is the gradient of the electron density.

The combination of RDG with the second eigen value of the Hessian matrix of the electron density, denoted as λ_2, allows for a more nuanced understanding of NCI. In these scatter plots, the RDG is plotted against the sign of the second Hessian eigen value multiplied by the electron density, sign(λ_2)ρ[27]. This representation provides clear visual indicators of the interaction types:

i) $\lambda_2\rho > 0$ (Red Regions): These regions indicate repulsive or steric interactions, where the electron density repels rather than attracts. This phenomenon is typically observed in regions of high electron density, where atoms or groups are in close proximity but do not interact favorably.

(ii) $\lambda_2\rho < 0$ (Blue Regions): These regions are indicative of attractive interactions, such as hydrogen bonds, where there is a significant directional attraction between electron-donating and electron-accepting sites.

B

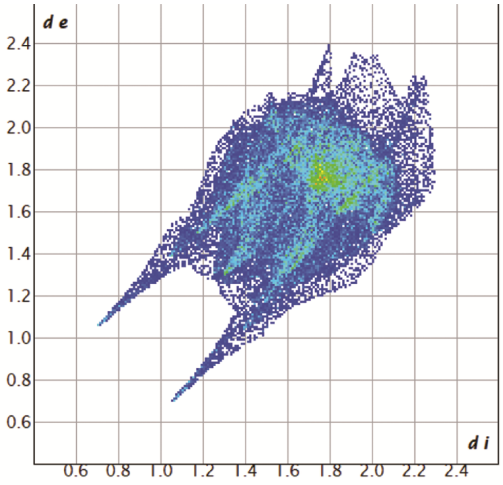

(a) All (100%)

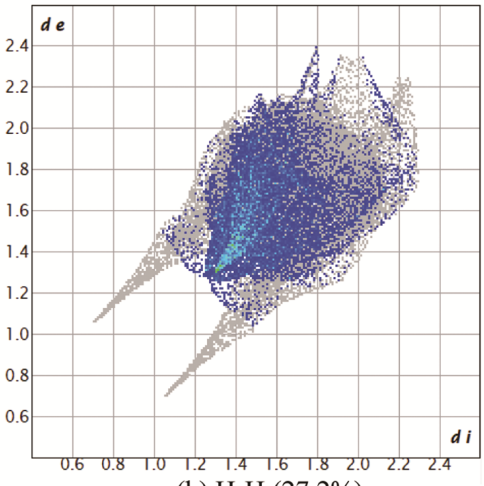

(b) H-H (27.2%)

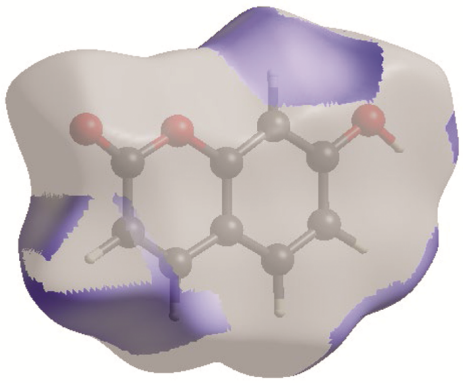

(b) d_{norm}-H-H (27.2%)

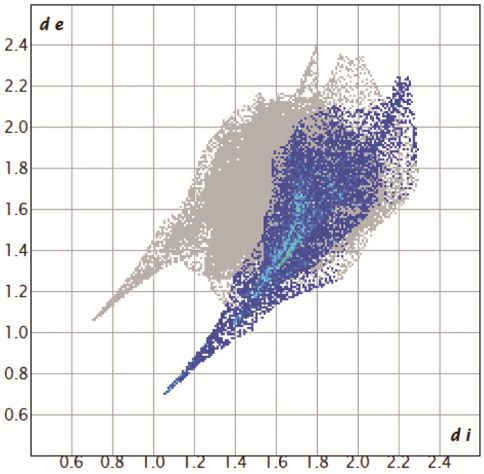

(c) O-H (22.8%)

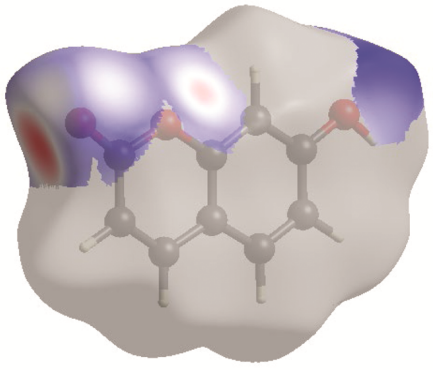

(c) d_{norm}-O-H (22.8%)

Fig. 7B — The 2D fingerprint plots for significant contacts of Antioxidant, C4 (A) (100% contribution); (B) H - H (27.2% contribution); (C) O-H (22.8% contribution) (*Contd*.)

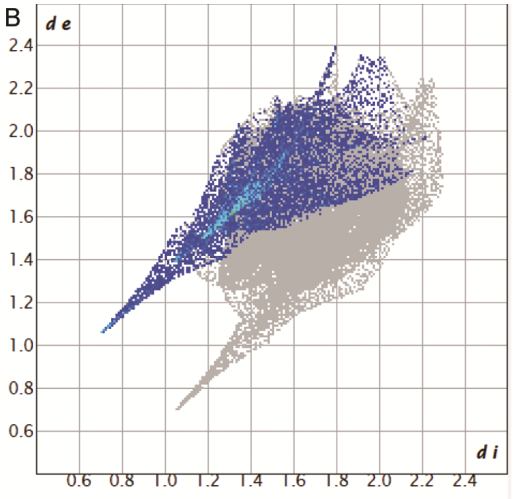

(d) H-O (18.6%)

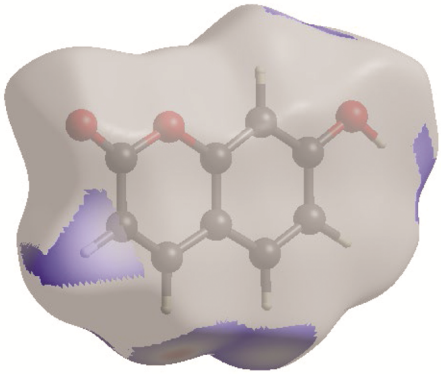

(d) d_{norm}-H-O (18.6%)

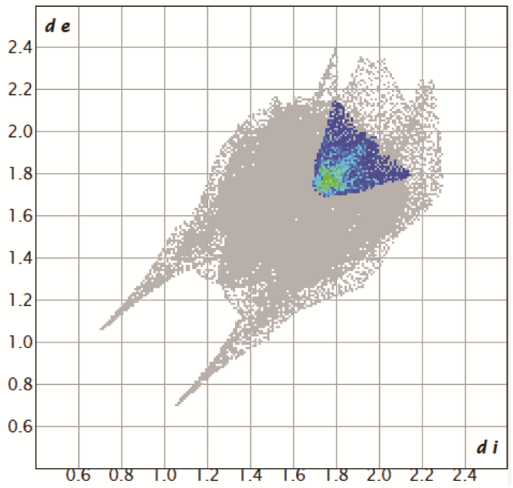

(e) C-C (11.2%)

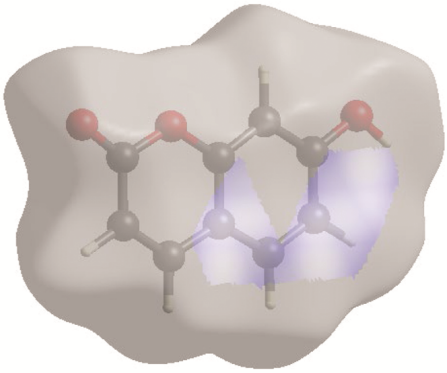

(e) d_{norm}-C-C (11.2%)

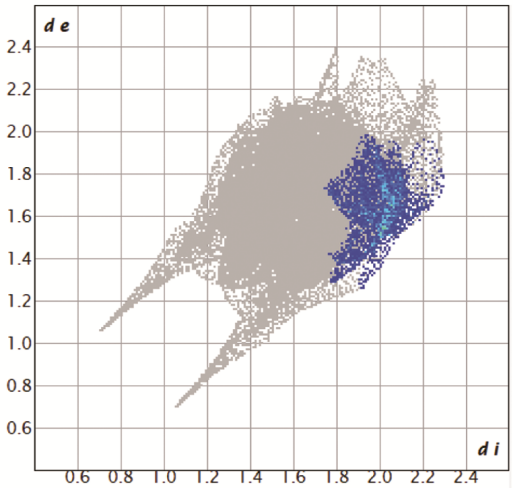

(f) C-H (8.9%)

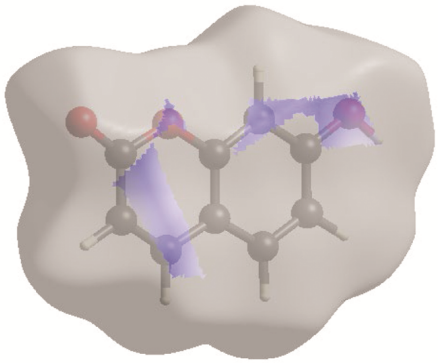

(f) d_{norm}- C-H (8.9%)

Fig. 7B — The 2D fingerprint plots for significant contacts of Antioxidant, C4 (D) H-O (18.6% contribution); (E) C-C (11.2% contribution); (F) C-H (8.9% contribution) (*Contd.*)

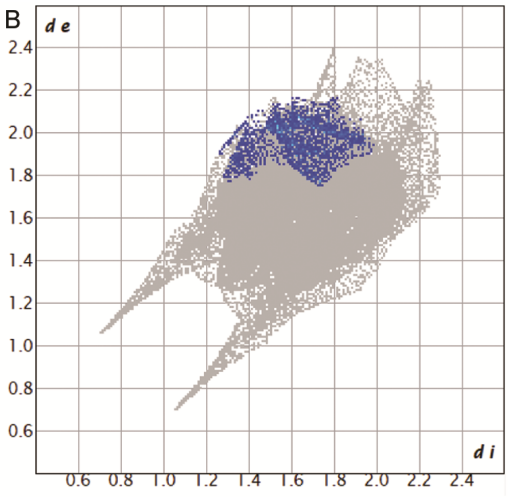

(g) H-C (5.2%)

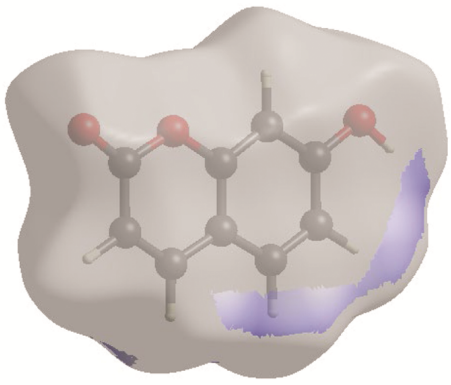

(g) d_{norm}- H-C (5.2%)

Fig. 7B — The 2D fingerprint plots for significant contacts of Antioxidant, C4 (G) H-C (5.2% contribution)

(iii) $\lambda_2\rho \approx 0$ (Green Regions):These regions denote weak vdW interactions, which are characterized by non-directional, relatively weak attractions between molecular fragments.

In the visualization and interpretation part, the NCI scatter diagram produces a stiletto heel-shaped plot, where distinct spikes at low densities correspond to various interaction types. These spikes offer a clear fingerprint for identifying the nature of interactions within the complex: i) vdW Interactions (Green Spikes): These are typically observed as small spikes around $\lambda_2\rho \approx 0$, indicating weak, non-directional attractions that stabilize the complex, ii) Hydrogen Bonds (Blue Spikes): These appear as prominent spikes where $\lambda_2\rho < 0$, reflecting strong, directional interactions between hydrogen donors & acceptors and iii) Steric Hindrance (Red Spikes): These are shown as sharp spikes where $\lambda_2\rho > 0$, signifying regions where electron clouds overlap, leading to repulsive interactions.

For the antioxidant C4, interacting with RO$^{\bullet}$ and HOO$^{\bullet}$ radicals, the 2D NCI scatter plots highlight dominant interactions as compared to other antioxidants (Fig. 8A). The RDG versus sign(λ_2)ρ plot for these complexes shows distinct fingerprints of vdW interactions, characterized by the prominence of green regions, as depicted in (Fig. 8A and Suppl. Fig. 3). This indicates that in presence of either hydrogen bonding or steric hindrance, the stabilization of the complex is primarily attributed to weak or non-directional forces.

Additionally, the 3D colour-filled isosurface, generated by using Visual Molecular Dynamics (VMD) is illustrated in (Fig. 8B and Suppl. Fig. 4). In the case of the C4 antioxidant interacting with RO$^{\bullet}$ and HOO$^{\bullet}$ radicals, green patches on the 3D RDG isosurface indicate weak vdW interactions. By analyzing the colours on the RDG isosurface, distinct interaction regions can be identified. Small red rings represent areas of electron density depletion caused by electrostatic repulsion, while the green patches, often mapped in green or light brown, highlight vdW interaction regions associated with low electron density. This suggests that these interactions contribute to the compound's stability, as lower electron density corresponds to reduced reactivity and enhanced stability. Thus, VMD analysis not only identifies specific interaction types but also provides insights into their role in the stability and chemical behavior of C4 antioxidant.

The Topological analysis of the Electron Localization Function (ELF) offers a sophisticated mathematical framework for characterizing chemical bonds, providing insights into the distribution and nature of electron density within molecules[28]. In Figure 8C, shaded surface maps with projection effects of the ELF are presented, employing a colour scheme to signify different levels of electron localization. Herein, strong electron localization is depicted by red and orange colours on the surface map, highlighting regions where electron density is highly concentrated. Specifically, red circles denote depletion regions between inner shell and valence shell interactions, emphasizing areas of significant electron localization. In contrast, the ELF colour-filled

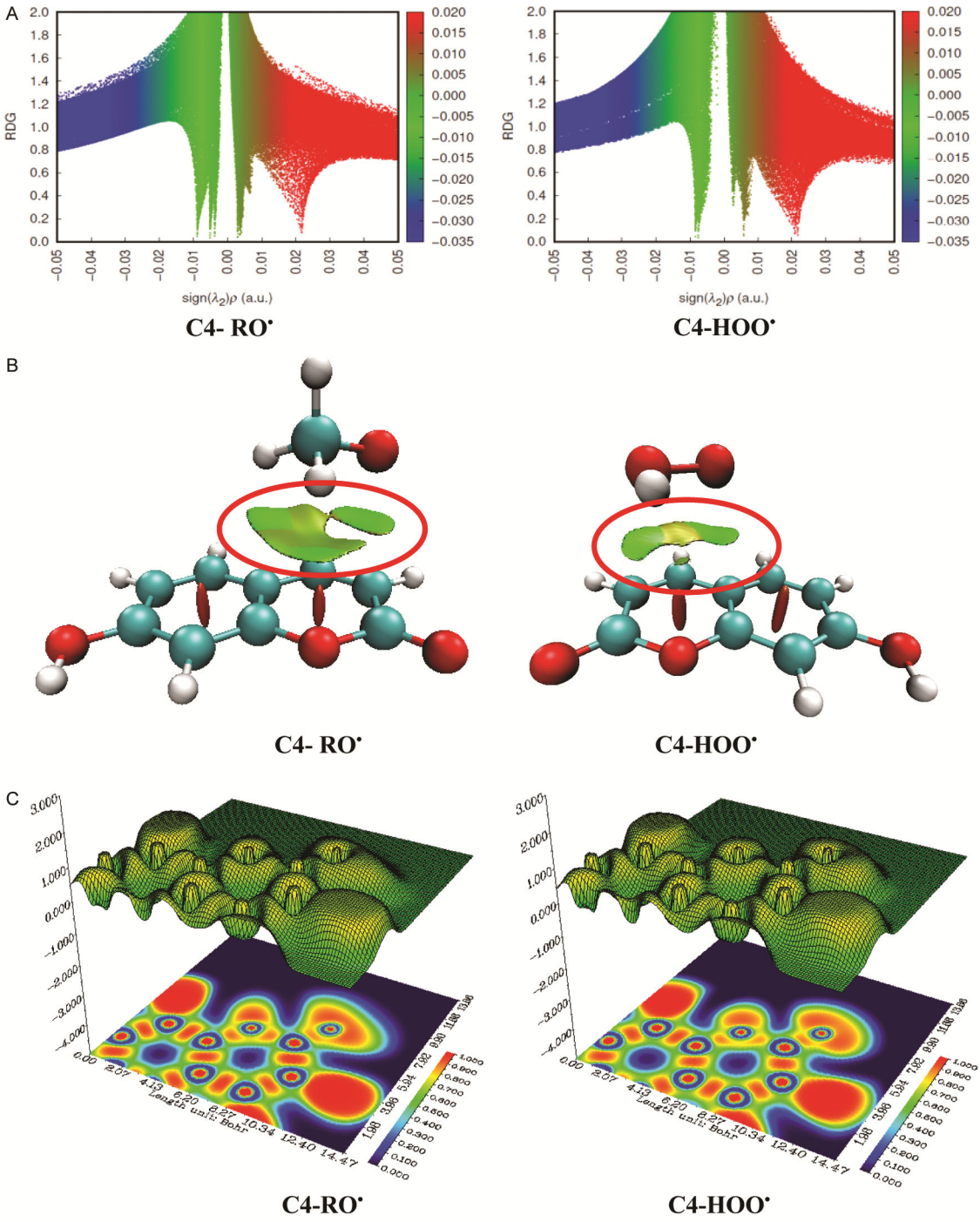

Fig. 8 — (A) NCI plots of the minimized models of Antioxidant C4 with RO•/HOO• radicals; (B) VMD plots of the minimized models of Antioxidant C4 with RO•/HOO• radicals; and (C) ELF plots of the minimized models of Antioxidant C4 with RO•/HOO• radicals

map in (Fig. 8C) reveals blue regions around certain carbon and oxygen atoms, indicating delocalized electron clouds. This characterization underscores the presence of areas where electrons are more diffusely spread out, suggesting less localized bonding compared to the red and orange regions. The areas surrounding hydrogen atoms prominently display localized bonding features, reflecting specific interactions where electrons are tightly bound within the vicinity of these atoms. Again, non-bonding electrons are distinctly marked by the red colour, signifying regions where electrons are not involved in

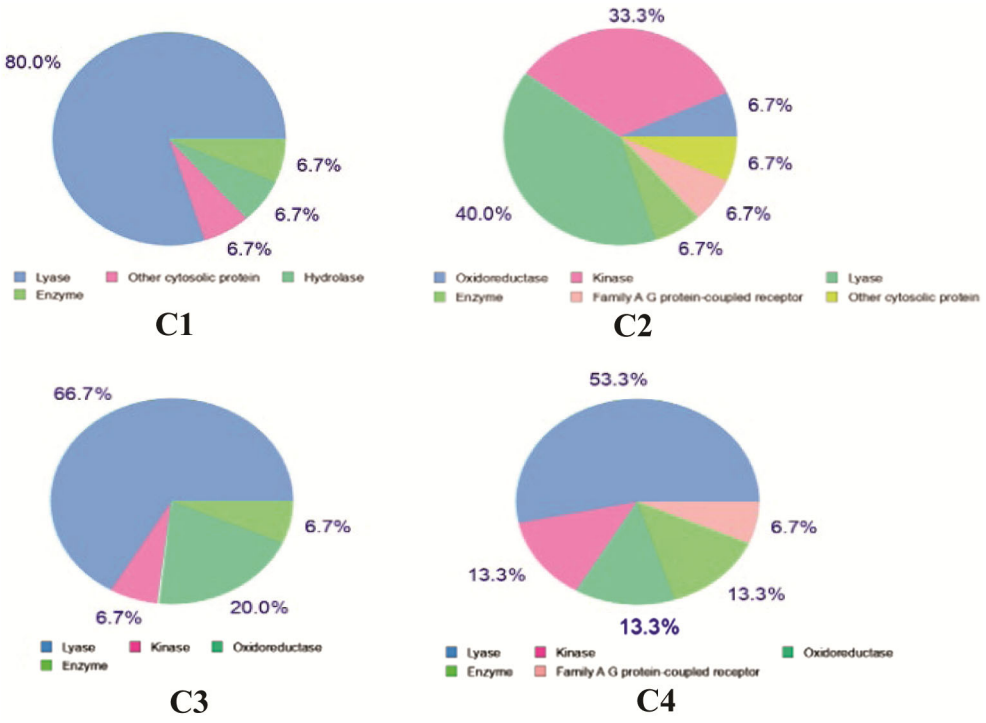

Fig. 9 — The target predication for Antioxidants C1, C2, C3 and C4

bonding interactions, but are part of localized orbital environments. This detailed analysis, employing advanced visualization techniques of the ELF, contributes significantly to our understanding of molecular structure and bonding patterns; enhancing our ability to interpret the chemical properties and interactions.

Protein Target Prediction for coumarin derivatives

Swiss Target Prediction uses a ligand-based similarity approach to predict protein targets for small molecules; based on the principle that similar molecules are likely to bind with similar targets. This tool usually compares a query molecule to a database of known bioactive molecules to identify potential protein targets. Swiss Target Prediction determines the most similar molecules in its database and predicts the most likely targets for the query molecule, using a dataset of 100 entries[29].Coumarin and its derivatives *i.e.*, C2, C3 and C4 demonstrated high probabilities of binding to lyases with 80%, 40%, 66.7% and 53.3%, respectively, as shown in (Fig. 9). Among the top 15 predicted protein targets, CA VII (PDB ID: 3ML5) was selected for our analysis.

Ramachandran plot

The Ramachandran plot is widely used to evaluate the structural stability and stereochemical quality of

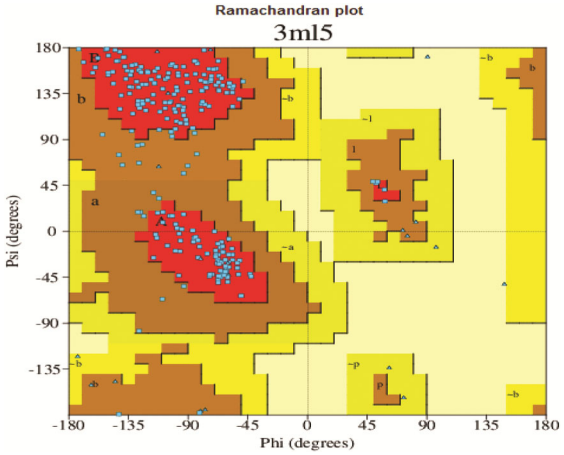

Fig. 10 — Ramachandran plot for the protein CA VII

the protein's 3D conformation[30]. Herein, the structural integrity, reliability and stability of CA VII protein can be assessed by using the plot as illustrated in (Fig. 10). The red areas of the plot signify the most favored regions, brown areas indicate allowed regions and yellow areas represents disallowed regions, with exceptions for residues like glycine and proline. The Ramachandran plot generated by PDBsum shows 87.8% of residues in the most favoured regions, 12.2% in the allowed regions and 0% in the disallowed regions, indicating a reliable structure for CA VII.

Table 8 — Summary of the bound amino acid, binding energy, bond distance between the target (CA VII) and ligands (C1, C2, C3 and C4), different types of interactions, aromaticity, hydrophobicity, hydrogen bond, ionisability, charge and solvent accessible surface

Compounds	C1	C2	C3	C4
Residues	THR A:199; VAL A:121; VAL A:143; HSD A:94	THR A:199; VAL A:121	TRP A:209; VAL A:143; LEU A:198; GLN A:67; THR A:199; HSD A:94	VAL A:121; LEU A:198; HSD A:94; THR A: 200
Affinity (kcal/mol)	-5.20	-5.38	-5.32	-5.45
Bond Distances (Å)	1.96; 5.05; 4.85; 5.56; 3.97	1.75; 1.79; 5.28	4.65; 4.53; 5.06; 2.04;1.71; 1.86; 5.00	5.25; 5.12; 4.10; 2.16
ConventionalHydrogen Bond	THR A: 199	THR A:199; THR A:199	GLN A:67; THR A:199; THR A:199	THR A:200
π Donor Hydrogen Bond	HSD A:94	-----	-----	HSD A:94
π - π T Shaped	HSD A:94	-----	-----	-----
π - π Stacked	-----	-----	HSD A:94	-----
π -Alkyl	VAL A:121; VAL A:143	VAL A:121	TRP A:209	VAL A:121; LEU A:198
Alkyl			VAL A:143; LEU A:198	
Aromaticity (Yes/No)	Yes	Yes	Yes	Yes
Hydrophobicity (Yes/No)	Yes	Yes	Yes	Yes
Hydrogen bond (Yes/No)	Yes	Yes	Yes	Yes
Ionisability (Yes/No)	No	No	No	No
Charge (Yes/No)	No	No	No	No
Solvent Accessible surface (Yes/No)	Yes	Yes	Yes	Yes

Molecular docking analysis

Molecular docking method provides a platform to predict the binding affinity and orientation of ligands within the binding pockets of receptors, a crucial step in understanding the molecular basis of biological processes[31]. The minimal binding affinities, considering hydrogen bonding, hydrophobic and electrostatic interaction and vdW forces of ligand-protein binding complexes; alongside the ligand efficacies of small molecules against target substrates, were computed using the SeamDock tool[32]. Comprehensive analysis and visualization of ligand-receptor interactions, along with their docking poses, were performed using BIOVIA Discovery Studio software[33].

Molecular docking was performed to evaluate the potential of selected coumarin derivatives as inhibitors of CA VII (PDB ID: 3ML5). The ligand-protein interaction reveals that coumarin derivatives preferably interacts with amino acid residues of enzyme *viz*. THR A:199, THR A:200, VAL A:121, VAL A:143, HSD A:94, LEU A:198, TRP A:209 and GLN A:67 as depicted in (Table 8 and Fig. 11), where hydrogen bonding and other vdW interactions *i.e.*, hydrophobic π-alkyl, π-π stacking, π-donor *etc*. are found to be the most prominent. Particularly, THR A:199 residue shows strong hydrogen bonding interaction with benzopyrone ring or other moieties of the coumarin derivatives; where α-pyrone ring of C1 interacts with THR A:199 residue at hydrogen bond length of 1.96 Å; again, two -OH groups of C2 interacts with THR A:199 residue to form two hydrogen bonds with bond lengths of 1.75 and 1.79 Å. Interestingly in C3, α-pyrone ring and two -OH groups interact with two protein residues *i.e.*, GLN A: 67 and THR A:199 to form three strong hydrogen bonds with bond lengths of 2.04, 1.86 and 1.71 Å respectively. But, C4 engages only one hydrogen bonding interaction with THR A:200 at bond length of 2.16 Å. Besides H-bonds, various non-covalent interactions are observed in the minimized docked complexes. For example: a) α-Pyrone rings of C1 and C4 interacts with HSD A:94 residue of protein through π-donor H-interactions, b) Benzene ring of C1 and HSD A:94 residue shows very weak π-π T-shaped interaction, c) α-Pyrone ring of C3 engages in π-π stacking interaction with HSD A:94 residue, d) Benzene rings of C1, C2 and C4 involves π-alkyl interactions with VAL A:121 residue, e) benzene rings of C3 involves poor alkyl interactions with VAL A:143 and LEU A:198 residues, f) VAL A:143 and LEU A:198 engages π-alkyl interaction with the pyrone ring of C1 and the benzene ring of C4 and g) TRP A:209 residue and the hydroxyl group of C3 alone establishes a π-alkyl interaction (Fig. 11). Hence, our docking study clearly reveals that C4 has a

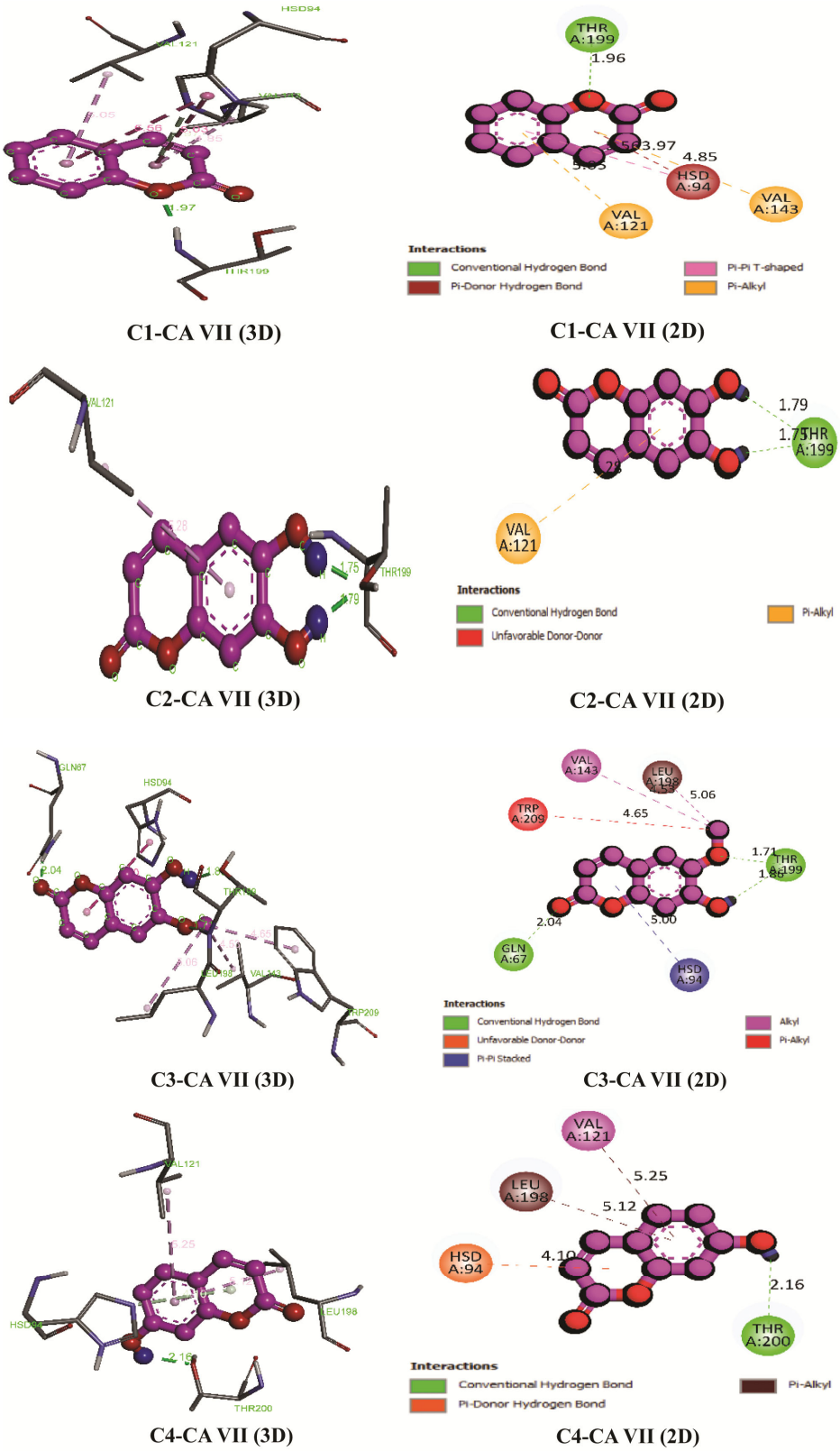

Fig. 11 — 3D and 2D binding mechanism of Antioxidants C1, C2, C3 and C4 with Protein residue of CA VII

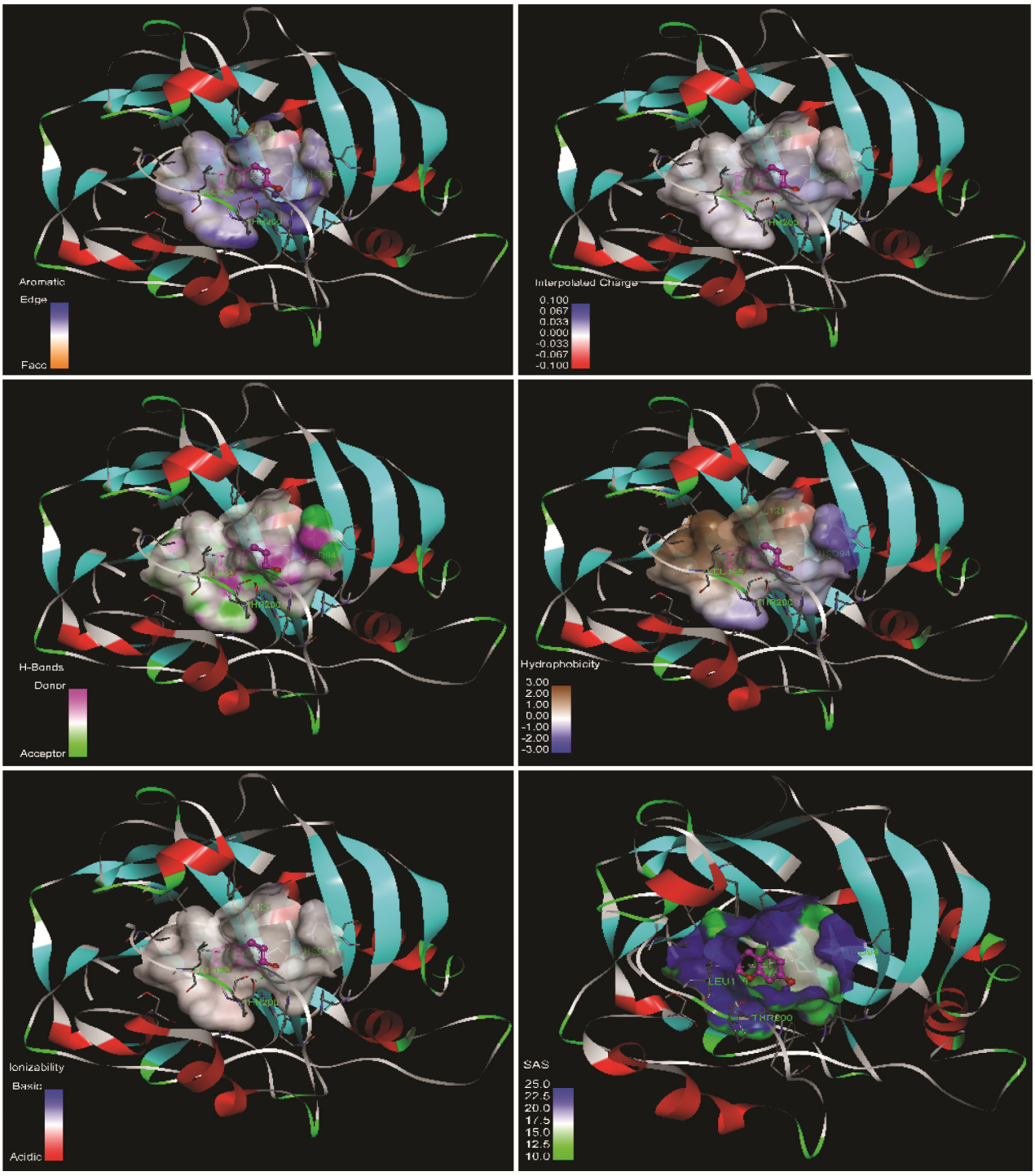

Fig. 12 — Different binding modes of Antioxidant C4 with CA VII, in case of aromaticity, charge, Hydrogen bonds, hydrophobicity, ionizability and solvent accessible surface

better binding affinity compared to other coumarin derivatives, as indicated by the observed trend in their docking scores; where C4 showing the highest binding affinity of -5.45 kcal/mol in comparison to others *i.e.*, C1, C2 and C3 with binding affinity values of -5.20, -5.38 and -5.32 kcal/mol respectively as shown in (Table 8). Since, C4 retains a neutral charge state; it may have a wider range of antioxidant activity than ionizable molecules as displayed by (Fig. 12). The hydrophilic -OH group of C4 deliberately forms

hydrogen bonds, facilitating interactions with the Zn^{2+} of CA VII protein; additionally, the large solvent-accessible surface may also contribute to reduce the generation of free radicals. Hence, this result supports that C4 is a particularly strong antioxidant among the studied coumarins, because of its significant physicochemical characteristics as shown in (Fig. 12).

Physicochemical and drug-likeness property analysis

Different physicochemical properties of the coumarin derivatives *viz*., molecular weight values, no. of H-bond acceptors (nHA) and donors (nHD), rotatable bonds (nRot), formal charge (fchar), topological polar surface area (TPSA), molar refractivity (MR), aqueous solubility (logS), octanol-water partition coefficient (logP) and distribution coefficient (logD), can be evaluated by using ADMETlab 2.0 or 3.0 virtual web tool laboratories[34]. Similarly, other therapeutic parameters such as quantitative estimate of drug-likeness (QED), fraction of sp^3 carbons (Fsp^3), medical chemistry evolution (MCE-18), Lipinski's rule of five (RO5), Pfizer rule, GlaxoSmithKline (GSK) rule, golden triangle rule, Pan assay interference compounds (PAINS), ALARM NMR and chelators are also very significant for analyzing the efficacy of drug like agents[35].

A thorough overview of the physicochemical characteristics of antioxidants illustrating molecular weight, nHA, nHD, nRot, fchar, TPSA, MR, logS, logP, logD, number of rings (nRing), maximum number of rings (MaxRing) and number of hetero atom (nHet); are incorporated in the radar chart as depicted in (Table 9 and Fig. 13). Coumarin derivatives comply with Lipinski's rule of five; indicating their potential for favorable oral bioavailability as promising drug candidates. The molecular weights of C1, C2, C3 and C4 are found to be 146.00, 178.00, 192.00 and 162.00 g/mol respectively, which fall within the optimal range of 100-600 g/mol. The nHA values for C1, C2, C3 and C4 are 2, 4, 4 and 3, respectively (optimal range: 0-12), while the nHD values are found to be 0, 2, 1 and 1 (optimal range: 0-7). Notably, C3 is the only compound with a nRot, within the optimal range of 0-11. The computed TPSA, MR, nRot, fChar, logS, logP and logD values for these molecules also fall within the optimal range, highlighting their potential as the most promising antioxidant candidates as depicted in (Table 9). In addition, the radar chart generated by using SwissADME for common physicochemical properties, including flexibility, unsaturation, solubility, lipophilicity, polarity and size, refers that these coumarin derivatives fall within the favourable range (with the pink zone) for oral bioavailability, except for instauration, which lies outside the pink zone, as shown in (Fig. 14).

The medicinal chemistry profiles for the antioxidants are summarized in (Table 10). Each compound achieves a QED score of 1, indicating ideal drug-likeness properties, with an optimal QED score is considered to be above 0.67. Nevertheless, all compounds adhere to RO5 ($MW \leq 500$, $logP \leq 5$, $Hacc \leq 10$, $Hdon \leq 5$), suggesting good absorption and permeability. Additionally, they conform to the Pfizer rule ($logP > 3$ and $TPSA < 75\ A^2$) and the GSK rule ($MW \leq 400$; $logP \leq 4$) which supports favorable ADMET profiles. However, none of the derivatives align with the Golden Triangle rule parameters ($200 \leq MW \leq 500$ and $-2 \leq logD \leq 5$). In these coumarin derivatives, it has been observed that three out of four rules perfectly follow the drug likeness properties indicating good oral bioavailability and absorption. Hence, they may be considered as better antioxidants. Furthermore, Figure 15 illustrates the drug-likeness behaviour scores for the coumarin derivatives, which are -1.05, -1.22, -1.23 and -0.65, respectively; as predicted by using Molsofttool[36]. Our analysis reveals that C4 exhibits the most favourable drug-likeness behaviour, falling within the acceptable range of -6 to

Table 9 — Physicochemical properties of Coumarin derivatives

Compound	MW (g/mol)	nHA	nHD	TPSA (A^2)	MR	nRot	fChar	logS	logP	logD
C1	146.00	2	0	30.00	43.00	0	0	-2.00	2.00	1.51
C2	178.00	4	2	71.00	47.00	0	0	-2.00	1.00	0.80
C3	192.00	4	1	60.00	51.00	1	0	-2.00	1.00	1.00
C4	162.00	3	1	50.00	45.00	0	0	-2.00	1.31	1.25

*Molecular weight (MW), No. of hydrogen bond acceptors (nHA) and donors (nHD), Topological polar surface area (TPSA), Molar refractivity (MR), No of rotatable bonds (nRot), Formal charge (fChar), Aqueous solubility (logS), Partition coefficient (logP), logD: LogP at normal physiological pH

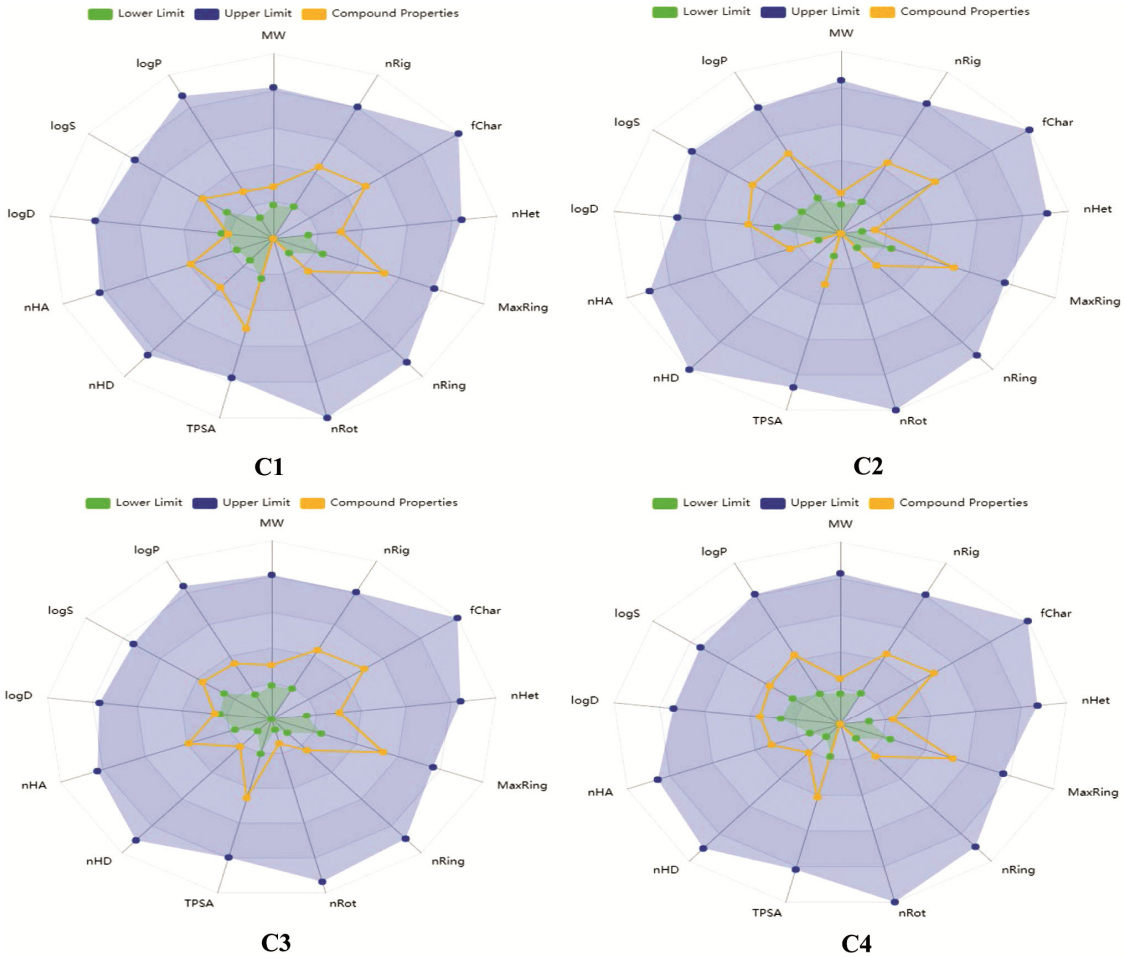

Fig. 13 — Radar chart depicting the physicochemical properties of C1, C2, C3, and C4 antioxidants. The bluish region represents the upper acceptable limits, the greenish region indicates the lower acceptable limits, and the brown lines correspond to the specific parameters of each compound, as evaluated using ADMETlab 3.0

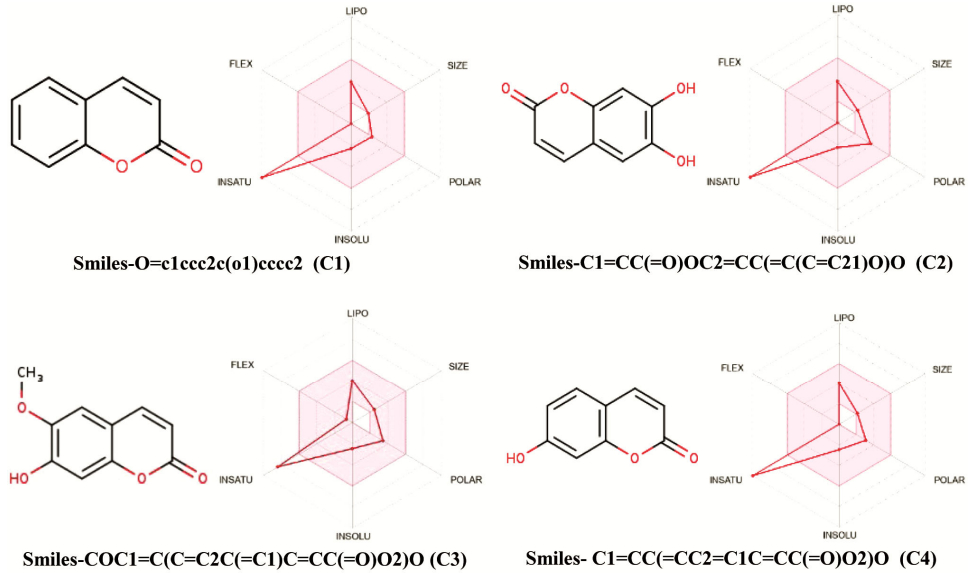

Fig. 14 — Oral bioavailability Radar chart for Antioxidants C1, C2, C3 and C4

Table 10 — Medicinal chemistry parameters of selected Coumarin derivatives

Compound	QED	Lipinski Rule	Pfizer Rule	GSK Rule	Golden Triangle Rule	PAINS	ALARM NMR	Chealator Rule
C1	1.00	Accept	Accept	Accept	Reject	0 Alerts	1	0
C2	1.00	Accept	Accept	Accept	Reject	1 Alerts	3	1
C3	1.00	Accept	Accept	Accept	Reject	0 Alerts	3	1
C4	1.00	Accept	Accept	Accept	Reject	0 Alerts	2	0

** Quantitative estimate of drug-likeness (QED), GlaxoSmithKline (GSK) and Pan assay interference compounds (PAINS)*

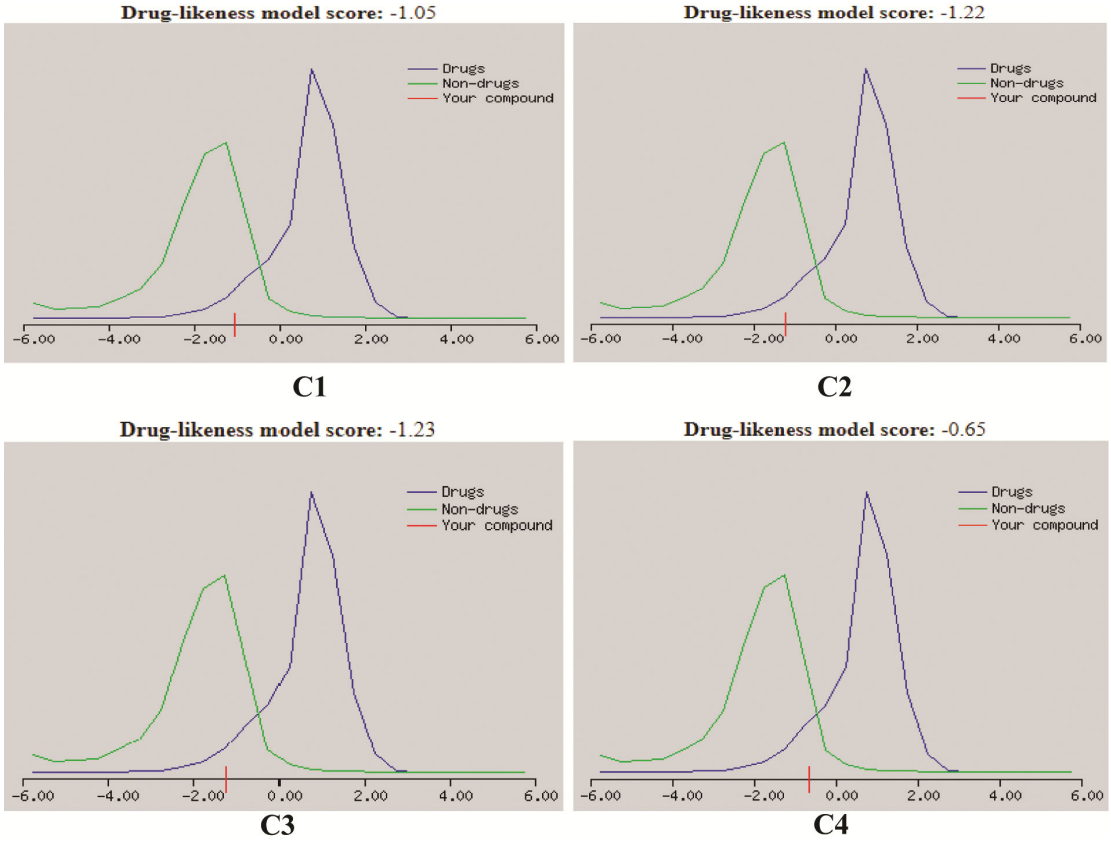

Fig. 15 — Plotting of the drug-likeness score of C1, C2, C3 and C4 using MolSoft. Non-drug-like behavior (green curve) and drug-like behavior (blue curve)

6. In terms of PAINS alerts, except C2; C1, C3 and C4 do not show any alerts indicating they are not frequent hitters, alpha-screen artifacts or reactive compounds as shown in (Table 10). On the other hand, C2 and C3 have shown three ALARM NMR alerts, while C1 and C4 have one and two ALARM alerts, respectively. This computational assessment also reveals that compounds C1 and C4 are non-chelating and non-reactive, while compounds C2 and C3 are chelating and reactive (Table 10).

Pharmacokinetic analysis

The pharmacokinetic, ADMET profile analysis *i.e.*, absorption, distribution, metabolism, excretion and toxicity; of the selected compounds may also be carried out for understanding their mechanism of action in relation to their antioxidant properties[37]. For absorption assessment, key parameters such as Caco-2 cell permeability, Human Intestinal Absorption (HIA), the role of compounds as P-glycoprotein (P-gp) inhibitors and bioavailability were predicted. The BOILED-Egg model from the SwissADME database was also utilized to get the refined absorption predictions. Again, the plasma protein binding (PPB), volume of distribution (Vd), blood-brain barrier (BBB) permeability and unbound plasma fraction (Fu) were also investigated to evaluate the detailed distribution properties. For analyzing the metabolic profiling, we focused on the

interaction of coumarin derivatives with the CYP450 microsomal enzyme system to identifying specific CYP450 subtypes involved in their biotransformation. Excretory parameters such as clearance (CL) and half-life ($t_{1/2}$), provide insight into the elimination of compounds from the host. Finally, comprehensive toxicity profiles were derived using ADMETlab 2.0, predicting several key toxicological endpoints, including hERG cardiotoxicity, human hepatotoxicity, drug-induced liver injury (DILI), AMES mutagenicity, rat acute oral toxicity, skin sensitization, carcinogenicity and eye irritation[38].

a) Absorption

Herein, the computed Caco-2 cell line permeability scores for the antioxidants C1, C2, C3 and C4 were found to be -5.00, -5.00, -5.00 and -4.80 cm/s respectively, higher than that of the optimal score of -5.15 Log units (Table 11). All antioxidants were found to be non-substrates of P-gp and predicted to have low HIA *i.e.*, < 30%, as shown in (Table 11). The bioavailability of all compounds exceeded 30%, except for C3, which was found to be within the range of 20-30%. Again, we also analyzed the absorption properties of the coumarin derivatives using BOILED-Egg graph as shown in (Fig. 16). In this model, compounds with high HIA appear in the egg white region, those capable of CNS penetration in the egg yolk region and non-oral absorption in the gray area. Based on our predictions, all antioxidants are likely to be absorbed *via* the intestinal route and cross the BBB, with an exception of C2. Among the investigated compounds, C4 stands out as the most favorable candidate due to its optimal permeability score of -4.80 cm/s, which is closer to the ideal permeability threshold *i.e.*, -5.15 cm/s, as compared to the other antioxidants (Table 11). Furthermore, C4 has the potential to cross the BBB and act as a P-gp inhibitor which enhances its efficacy and versatility. Despite low HIA, the high predicted bioavailability (> 30%) suggests strong potential for effective systemic exposure, making C4 as a promising candidate for further study.

b) Distribution

In distribution profile, the computed PPB values for antioxidants *i.e.*, C1, C2, C3 and C4 are found to be 87.00%, 85.00%, 84.00% and 85.70%, respectively as depicted in (Table 11); which are ideally found to be below 90% to avoid reduced therapeutic effects and in our case all compounds met this criterion. But, C4 in particular, has a high Vd value of 1.00 L/kg, placing it comfortably within the optimal range of 0.04-20 L/kg; comparable to C1, C2 and C3, which have low Vd values *i.e.*, 0.83, 0.49 and 0.69 L/kg, respectively (Table 11). Again, the computed Fu values for C2, C3 and C4 were found to be 19.00%, indicating a potentially more effective pharmacological profile (Table 11). Consequently, among the studied compounds, C4 emerges as the most favorable antioxidant due to its balanced PPB, optimal Vd and significant Fu values.

c) Metabolism

Table 12 outlines the Cytochrome P450 (CYP450) subtypes (CYP1A2, CYP2C19, CYP2C9, CYP2D6 and CYP3A4) involved in the metabolism of each coumarin derivative and identifies the subtypes that can be inhibited by these compounds. Notably, C1 shows a high potential for inhibiting multiple CYP450 isoforms, especially CYP1A2 and CYP2C19, as presented in (Table 12). According to our predictions, C2 and C3 are likely to inhibit CYP1A2 and CYP2D6 isoforms; while C4 is anticipated to inhibit the CYP1A2, CYP2D6 and CYP3A4 isoforms (Table 12). Additionally, all four coumarin derivatives are predicted to serve as substrates for CYP1A2, CYP2C9 and CYP2D6. Based on this metabolic analysis, C4 emerges as the most favorable derivative due to its broader inhibitory profile, affecting three major CYP450 isoforms *i.e.*, CYP1A2, CYP2D6 and CYP3A4. Hence, C4 could have significant implications for drug metabolism and potential drug-drug interactions.

Table 11 — Absorption and distribution-related parameters of Coumarin derivatives (*via* ADMETlab)

Compound	Absorption						Distribution			
	Caco-2	P-gp-inhibitor	P-gp-substrate	HIA	$F_{20\%}$	$F_{30\%}$	PPB %	Vd	BBB	Fu %
C1	5.00	0.00	1.00	0.00	1.00	1.00	87.00	0.83	0.00	12.00
C2	-5.00	0.00	1.00	0.00	1.00	1.00	85.00	0.49	0.00	19.00
C3	-5.00	0.00	1.00	0.00	0.00	1.00	84.00	0.69	0.00	19.00
C4	-4.80	0.00	1.00	0.00	1.00	1.00	85.70	1.00	0.00	19.00

**Caco-2: Caucasian colon adenocarcinoma, P-gp: para-glycoprotein, HIA: human intestinal absorption, F20%: 20% bioavailability, F30%: 30% bioavailability, PPB: plasma protein binding, Vd: volume of distribution, BBB: blood-brain barrier, Fu: unbound fraction in plasma*

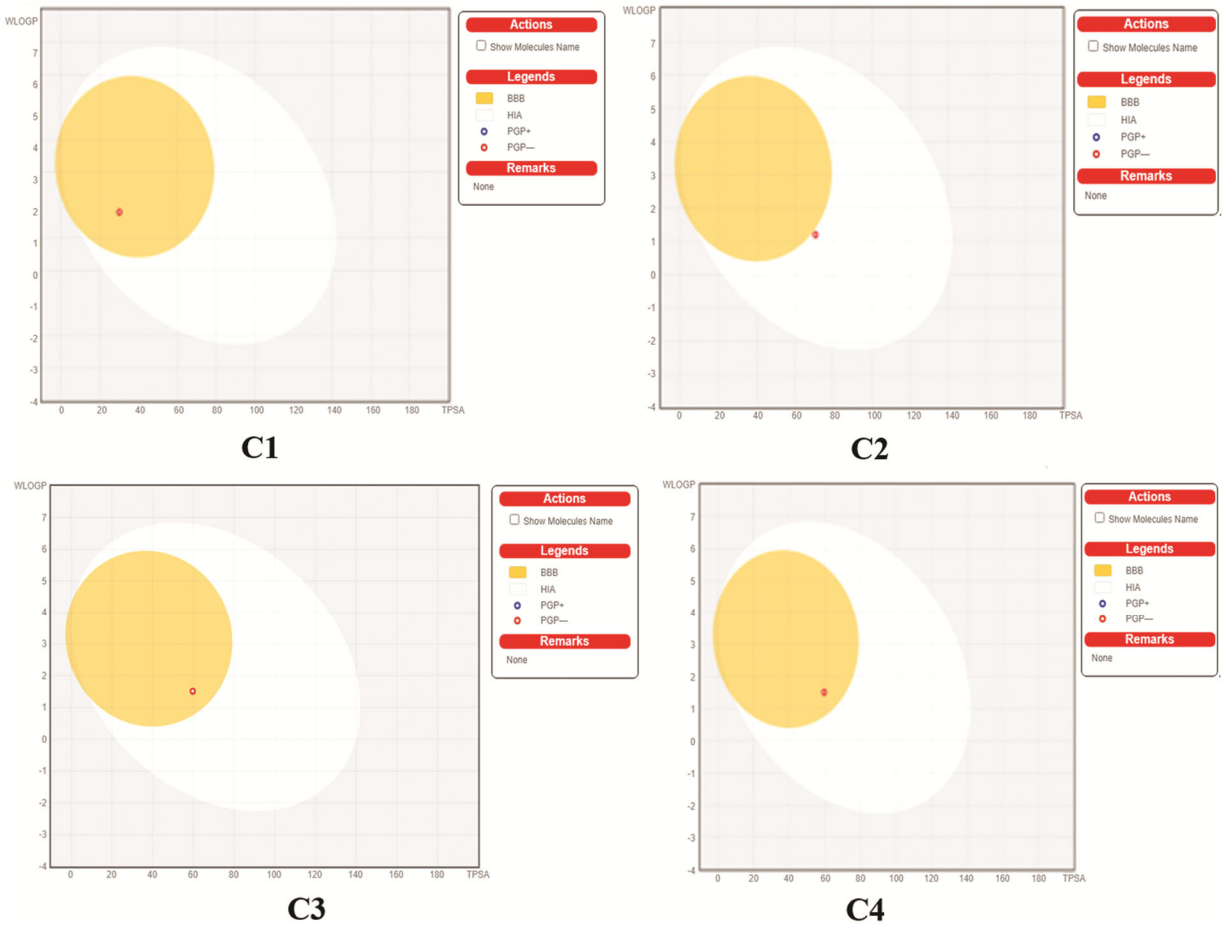

Fig. 16 — Graphical representation for C1, C2, C3 and C4 from the SwissADME using the BOILED-Egg method; BBB is denoted for blood-brain barrier, HIA for human intestinal absorption, PGP^+ for P-glycoprotein substrate, while PGP^- a non-P-glycoprotein substrate

Table 12 — Metabolism and excretion-related parameters of Coumarin derivatives (*via* ADMETlab)

Compound	Metabolism										Excretion	
	Inhibition of CYP 450 isoforms					Substrate of CYP 450 isoforms						
	1A2	2C19	2C9	2D6	3A4	1A2	2C19	2C9	2D6	3A4	$t_{1/2}$	CL
C1	1.00	1.00	0.00	0.00	0.00	1.00	0.00	1.00	1.00	0.00	1.00	11.00
C2	1.00	0.00	0.00	1.00	0.00	1.00	0.00	1.00	1.00	0.00	1.00	17.00
C3	1.00	0.00	0.00	1.00	0.00	1.00	0.00	1.00	1.00	0.00	1.00	13.00
C4	1.00	0.00	0.00	1.00	1.00	1.00	0.00	1.00	1.00	0.00	0.83	14.00

* *$t_{1/2}$: half-life, CL: clearance*

d) Excretion

In excretion profile, the computed CL rates for C1, C2, C3 and C4 were found to be 11, 17, 13 and 14 mL/min/kg, respectively as shown in (Table 12). C4 shows an efficient clearance rate of 14 mL /min/kg, placing it in the moderate excretion category per ADME guidelines (high: >15, moderate: 5-15, low: <5 mL/min/kg), indicating near-optimal excretion within this range. The predicted $t_{1/2}$ for C1, C2, C3 and C4 are 1, 1, 1 and 0.834 h, respectively, indicating that all these compounds have short half-lives (less than 3 h). Due to its nearly optimal CL rate and short $t_{1/2}$, C4 appears to be the most favorable excretion profile.

e) Toxicity

Both ADMETlab and the predhERG web server were consistent in evaluating hERG cardiotoxicity for these compounds[39]. The toxicity data for the antioxidants summarizing the predicted safety and efficacy characteristics are presented in (Tables 13 and 14).

Table 13 — Toxicity-related parameters of Coumarin derivatives (via ADMETlab)

Parameters	C1	C2	C3	C4
hERG Blockers	0.20	0.10	0.10	0.10
H-HT	0.10	0.10	0.20	0.10
DILI	1.00	1.00	1.00	0.70
AMES Toxicity	0.20	0.10	0.10	0.00
Rat Oral Acute Toxicity	0.70	0.10	0.10	0.40
Skin Sensitization	0.00	1.00	1.00	0.00
Carcinogenicity	1.00	1.00	1.00	0.80
Eye Corrosion	1.00	0.40	0.40	0.60
Eye Irritation	1.00	1.00	1.00	0.10

**Human hepatotoxicity (H-HT), drug-induced liver injury (DILI)*

Table 14 — Predicted Pred-hERG toxicity for Coumarin derivatives

Compounds	Prediction	Categorical potency	Potency (IC_{50})	Applicability domain
C1	Non-blocker	Moderator blocker	5.10	Inside
C2	Non-blocker	Weak-blocker	5.20	Outside
C3	Non-blocker	Weak-blocker	5.10	Outside
C4	Non-blocker	Non-blocker	5.00	Inside

Notably, ADMETlab predicted that none of the compounds exhibited hERG cardiotoxicity, aligning with the predhERG classification, categorizing all four compounds as non-cardiotoxic. The predhERG tool indicated that all four compounds were found to be non-blockers; however, distinctions among the compounds were noted, C1 was identified as a moderate blocker, C2 and C3 as weak blockers and C4 as a non-blocker, depicted in (Table 14). ADMETlab's assessment also highlights that, all the compounds exhibit a low tendency for human hepatotoxicity; while a predicted risk of DILI was observed for C1, C2 and C3; but no such risk was identified for C4. Additionally, all the compounds demonstrated negative AMES toxicity. Furthermore, C2, C3 and C4 exhibit low acute oral toxicity in rats. Regarding skin sensitization, C2 and C3 were identified as skin sensitizers and caused eye irritation, but not corrosion. In contrast, C1, a non-sensitizer, caused both eye irritation and corrosion, while C4, also a non-sensitizer, did not induce either eye irritation or corrosion. Among these compounds, carcinogenicity risk was high for C1, C2 and C3; whereas C4 possesses a low risk as shown in (Table 13); hence, C4 stands out as non-toxic across all evaluated parameters.

This lack of toxicity, coupled with a predicted IC_{50} value of 5.00, suggests a favorable ADMET profile for C4. The IC_{50} value reflects the compound's potency, specifically its antioxidant activity, which is a desirable attribute for therapeutic applications involving oxidative stress. Hence, C4 exhibits an exemplary safety profile, being non-toxic in all assessed parameters and demonstrates potential antioxidant activity, as evidenced by its IC_{50} value as depicted in (Table 14). As a result, C4 stands out as a promising candidate for ongoing development and application as an antioxidant in medicinal chemistry.

Molecular dynamics (MD) simulation

MD simulation was conducted using the Gromacs platform to assess the stability of CA VII in its bound state with the most preferred antioxidant, C4[40]. For execution, the protein-ligand complex was derived from the previous molecular docking results obtained using SeamDock. The parameter files were used to obtain the final structure of the molecules which was then solvated with TIP3P water molecules and the final system was mixed with Na^+ and Cl^- ions to maintain system polarity[41]. The solvated complex was set up in a truncated octahedron box ensuring a padding distance of 10 Å from the box's boundary. The OPLS2005 force field was used for protein topology, while the ligand was constructed using the SwissParam platform[42]. Initially, the complex was equilibrated for 5 ns in the NVT ensemble with a Berendsen thermostat at 310 K, followed by equilibration in the NPT ensemble using the Parrinello-Rahman barostat at 1 bars. This investigation aims to understand the extent of structural changes of the C4-CA VII complex over a 300 ns simulation period.

The stability of the complex was analyzed using statistical parameters like protein/ligand backbone Root Mean Square Deviation (RMSD), Root Mean Square Fluctuation (RMSF) of the constituent amino acid residues, Radius of Gyration (Rg) and intermolecular H-bonding of the complex. It was observed that the antioxidants interact near the Zn^{2+} ion of CA VII, which is located at the active site of metallo-protein. Thus, the statistical analysis of the MD simulation trajectory provides a brief analysis of the interacting behavior of the targeted complex. The mechanical behavior of the active site residues with respect to whole protein was observed using RMSD, RMSF, Rg and intermolecular H-bonds, as illustrated below:

i) RMSD value of the protein backbone is depicted in (Fig. 17). The X-axis depicts the time duration in

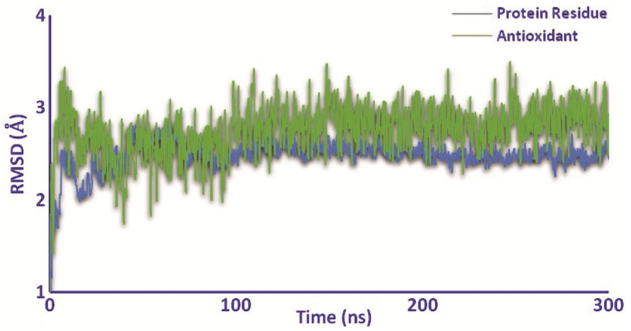

Fig. 17 — RMSD plots for antioxidant (C4)-Protein residue (CA VII) complex

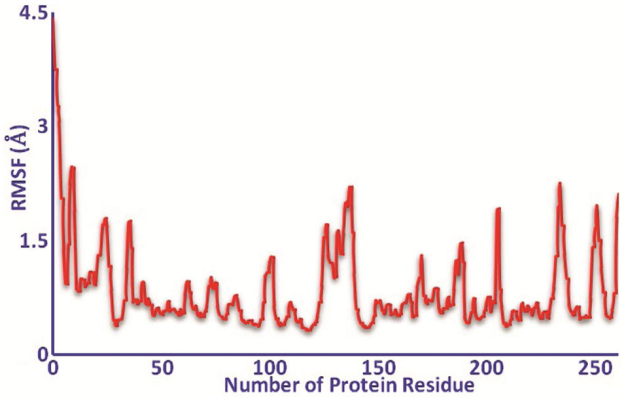

Fig. 18 — RMSF plot for Protein residues (CA VII) in the complex

ns, while the Y-axis depicts average displacement of the backbone atoms at a scale in Å. The trajectory is observed to rise at the initial frame to an extent of about 1.5 Å and later a gradual rise to 2.5 Å at time space of 50 ns. However, a trend towards stability is observed by forming a nearly straight-line trajectory with meager amplitude. The average RMSD of the complex was found to be 2.4 (± 0.18) Å; in comparison to the protein residue, the average RMSD of the ligand is found to be 3 (± 0.12) Å, which reflects a favorable C4-CAVII complex formation.

ii) RMSF values of the constituent protein residues were tallied over a time of 300 ns as depicted in (Fig. 18). Here, the X-axis depicts the residual position (number) and the Y-axis depicts average displacement of the C_α at a scale of Å. The average RMSF of the complex was found to be 0.85 (± 0.55) Å. It is noteworthy that the active site protein residues were found to be H94, V121, L198 and T200; which appears to correlate with the peaks observed in the RMSF plot. Hence, the cited protein residues are key to the C4-CAVII complex, as shown by the RMSF plot (Fig. 18).

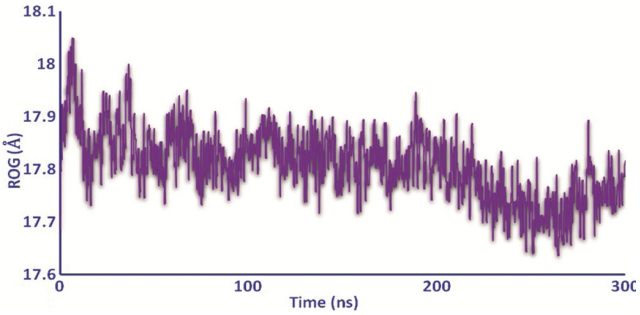

Fig. 19 — Rg plot for Antioxidant (C4)-Protein residue (CA VII) complex

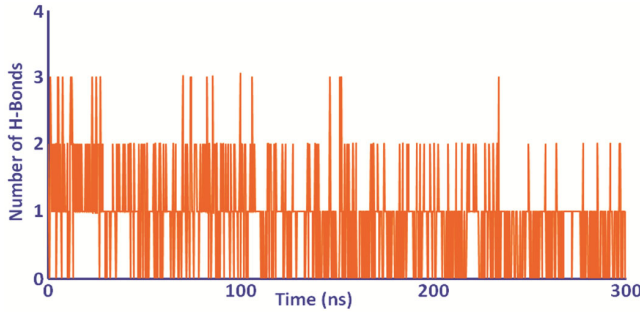

Fig. 20 — H-bonds plot for antioxidant (C4)-Protein residue (CA VII) complex

iii) The Rg plot of the C4-CAVII complex indicates the extent of compactness during its bound state. The observed Rg plot reflects a downward movement trend which strongly supports the stiffness between the protein and ligand with an average Rg of 18(± 0.06) Å, as shown in (Fig. 19).

iv) The intermolecular H-bond plot in (Fig. 20), depicts the interaction between C4 and interacting residues of the targeted protein. A normal H-bond is considered when a distance is found to be 2.8 Å between H-donor and H-acceptor entities. Herein, a maximum of 3 H-bonds was observed at different time frames, where two of them tend to be constant throughout the simulation.

Conclusion

The above findings provide a foundation for further exploration of structure-activity relationships and the development of novel antioxidant compounds based on the coumarin scaffold. The computational analysis amongst all the antioxidants revealed that only C4 *i.e.*, umbelliferone exhibits significantly higher binding affinities to the reactive radical species *i.e.*, $RO^{\bullet}$ and $HOO^{\bullet}$;whichindicates its potential antioxidant activity. The thermodynamic profile analysis of the C4-$RO^{\bullet}$/$HOO^{\bullet}$ radical complex further supports C4's

effectiveness as an antioxidant. The SET-PT mechanism is identified as the most favorable pathway, attributed to its efficient electron transfer capability followed by H^+ dissociation, thereby confirming its superior antioxidant efficacy. The DFT calculation is also very helpful for analyzing different electronic & physicochemical properties, spin density, charge distribution, chemical reactivity studies for the C4-$RO^{\bullet}$/$HOO^{\bullet}$ radical complexes. The Hirshfeld surface analysis, along with the corresponding 2D-fingerprint plots reveals that the antioxidant, C4 is primarily stabilized by H···H and O···H/H···O interactions. Further, molecular docking studies show that C4 exhibits the highest binding affinity with CA VII protein, forming hydrogen bonds and hydrophobic interactions with residues *viz*., THR A:200, HSD A:94, VAL A:121 and LEU A:198. Additionally, the physicochemical and drug-likeness evaluation parameters for C4 also fall within the optimal range. Moreover, ADMET analysis predicts that C4 shows quite favorable absorption (Caco-2, HIA, F30%), distribution (PPB, Vd and Fu), metabolism (CYP1A2, CYP2D6, CYP3A4), excretion (CL, $t_{1/2}$) and low toxicity risks, including non-carcinogenicity and non-mutagenicity. Finally, molecular dynamics simulation study also provides evidence that C4 is a highly promising antioxidant with significant therapeutic potential. It offers deeper insights into its exceptional radical-scavenging activity, stable interactions with biological targets, favourable pharmacokinetics and strong safety profile.

Acknowledgement

The author sincerely acknowledges the valuable support and facilities provided by the Department of Applied Sciences and the Department of Bioengineering and Technology, Gauhati University.

Conflict of interest

All authors declare no conflict of interests.

References

1 Qin D, Jiao L, Wang R, Zhao Y, Hao Y & Liang G, Prediction of antioxidant peptides using a quantitative structure-activity relationship predictor (AnOxPP) based on bidirectional long short-term memory neural network and interpretable amino acid descriptors. *Comput Biol Med*, 154 (2023) 106591.

2 Rahman MA, Islam MR, Faruque MA, Das A & Ahmed M, Recent advances in cellular signaling interplay between redox metabolism and autophagy modulation in cancer: an overview of molecular mechanisms and therapeutic interventions. *Antioxidants*, 12 (2023) 428.

3 Xu DP, Li Y, Meng X, Zhou T, Zhou Y, Zheng J & Li HB, Natural antioxidants in foods and medicinal plants: Extraction, assessment and resources. *Int J Mol Sci*, 18 (2017) 96.

4 Antropova IG, Revina AA, Kurakina ES & Magomedbekov EP, Radiation chemical investigation of antioxidant activity of biologically important compounds from plant materials. *ACS Omega*, 5 (2020) 59765983.

5 Abdoli M, Supuran CT & Žalubovskis R, 2-((1H-Benzo[d] imidazol-2-yl) amino) benzo[d] thiazole-6-sulphonamides: a class of carbonic anhydrase II and VII-selective inhibitors. *J Enzyme Inhib Med Chem*, 38 (2023) 2174981.

6 Lemon N, Nicole J, Bohndorf P, Tarantini MD & Wanner MP, Carbonic anhydrases as potential targets against neurovascular unit dysfunction in Alzheimer's disease and stroke. *Front Aging Neurosci,* 13 (2021) 772278.

7 Matos MJ, Coumarin and its derivatives. *Molecules*, 26 (2021) 6320.

8 Öztürk N, Özdemir T, Alpaslan YB, Gokce H & Alpaslan G, Experimental (FT-IR, Raman, and NMR) and theoretical (B3LYP, B3PW91, M06-2X, and CAM-B3LYP) analyses of P-tert-butylphenyl salicylate. *Bilge Int J Sci Technol Res*, 2 (2018) 5673.

9 Sharma S, Bezbaruah MJ, Ali I, Choudhury M & Bezbaruah B, Theoretical investigations on the π-π stacking interactions in phenol-water complexes. *Comput Chem*, 6 (2018) 1525.

10 Murail S, De Vries SJ, Rey J, Moroy G &Tufféry P, SeamDock: an interactive and collaborative online docking resource to assist small compound molecular docking. *Front Mol Biosci*, 8 (2021) 716466.

11 Vardhan S & Sahoo SK, *In silico* ADMET and molecular docking study on searching potential inhibitors from limonoids and triterpenoids for COVID-19. *Comput Biol Med*, 124 (2020) 103936.

12 Pratyashee B, Benzir A & Bipul B, SomePt (II)-complexes withdpb, Fdpband F2dpb ligandsas potent anticancer agents and their mode of interaction with AT/GC base pairs: A DFT study. *J Indian Chem Soc*, 100 (2023) 100923

13 Kaur C & Mandal D, The scavenging mechanism of aminopyrines towards hydroxyl radical: A computational mechanistic and kinetics investigation. *Comput Theor Chem*, 1219 (2023) 113973.

14 Milanović Ž, Dimić D, Avdović EH, Simijonović DM, Nakarada Đ, Jakovljević V & Marković ZS, Mechanism of Antiradical Activity of Coumarin-Trihydroxybenzohydrazide Derivatives: A Comprehensive Kinetic DFT Study. *Antioxidants*, 13 (2024) 143.

15 Zhang J &Rueping M, Metallaphotoredox catalysis for sp^3 C–H functionalizations through hydrogen atom transfer (HAT). *Chem Soc Rev*, 52 (2023) 40994120.

16 Chen M, Li Z, Sun G, Jin S, Hao X, Zhang C & Xue Y, Theoretical study on the free radical scavenging potency and mechanism of natural coumestans: Roles of substituent, noncovalent interaction and solvent. *Phytochem*, 207 (2023) 113580.

17 Molaei S, Dadkhah Tehrani A & Shamlouei H, Antioxidant activities of new carbohydrate-based gallate derivatives: A DFT study. *J Mol Liq*, 377 (2023) 121506.

18 Guin M, Mondal S, Roy S, Bhattacharyya S & Dey S, Synthesis and X-ray crystal structure of Cu(II) 1D coordination polymer: Hirshfeld surface, FMO, molecular

electrostatic potential (MEP) and natural bond orbital (NBO) analyses. *J Mol Struct*, 1270 (2022) 133949.

19 Zhang N, Wu Y, Qiao M, Yuan W, Li X, Wang X & Zi C, Structure–antioxidant activity relationships of dendrocandin analogues determined using density functional theory. *Struct Chem*, 33 (2022) 795.

20 Halim SA & Ibrahim MA, Synthesis, DFT calculations, electronic structure, electronic absorption spectra, natural bond orbital (NBO) and nonlinear optical (NLO) analysis of the novel 5-methyl-8H-benzo[h]chromeno [2,3-b][1,6]naphthyridine-6(5H),8-dione (MBCND). *J Mol Struct*, 1130 (2017) 543558.

21 Rouhani M, Evaluation of structural properties and antioxidant capacity of Proxison: A DFT investigation. *Comp Theor Chem*, 1195 (2021) 113096.

22 Singh N, Arish M, Kumar P, Rub A & Riaz U, Experimental and theoretical studies of novel azo benzene functionalized conjugated polymers: in-vitro antileishmanial activity and bioimaging. *Sci Rep*, 10 (57) (2020).

23 Steffy AD, Dhas DA, Joe IH & Balachandran S, Theoretical investigations on structural, spectral, NBO, NLO, and topology exploration (AIM, ELF, LOL, RDG) of piperazine-2,5-dione oxalic acid monohydrate. *J Mol Struc*, 1295 (2024) 136653.

24 Abad N, Lgaz H, Atioglu Z, Akkurt M, Mague JT, Ali IH, Chung IM, Salghi R, Essassi EM & Ramli Y, Synthesis, crystal structure, hirshfeld surface analysis, DFT computations and molecular dynamics study of 2-(benzyloxy)-3-phenylquinoxaline. *J Mol Str*, 1221 (2020) 128727.

25 Gannouni A, Tahri W, Roisnel T, Al-Resayes SI, Azam M & Kefi R, Single crystal investigations, Hirshfeld surface analysis, DFT studies, molecular docking, physico-chemical characterization, and biological activity of a novel non-centrosymmetric compound with a copper transition metal precursor. *ACS Omega*, 8 (2023) 77387748

26 García JC, Boto RA, Ruiz FI, Reva I, Woller T & Alonso M, A benchmark for the non-covalent interaction (NCI) index or… is it really all in the geometry?.*Theor Chem Acc*, 135 (2016) 242.

27 Saleh G, Gatti C, Presti L & Contreras-García J, Revealing Non-covalent Interactions in Molecular Crystals through Their Experimental Electron Densities. *Chem Eur J*, 18 (2012) 1552315536.

28 Tarika JDD, Dexlin XDD, Madhankumar S, Jayanthi DD & Beaula TJ, Tuning the Computational Evaluation of Spectroscopic, ELF, LOL, NCI Analysis and Molecular Docking of Novel Anti-COVID-19 Molecule 4-Dimethylamino Pyridinium 3, 5-Dichlorosalicylate. *Spectrochim Acta A Mol Biomol Spectrosc*, 259 (2021) 119907.

29 Daina A, Michielin O & Zoete V, SwissTargetPrediction: Updated data and new features for efficient prediction of protein targets of small molecules. *Nucleic Acids Res*, 47 (2019) 357364.

30 Laskowski RA, PDBsum: A standalone program for generating PDBsum analyses. *Protein Sci*, 31 (2022) 1.

31 Tahir MN, Ashfaq M, Dehnayebi MF, Munawar KS, Atalay S, Dege N, Guliyeva N & Sultan A, Crystal structure, Hirshfeld surface analysis, computational study and molecular docking simulation of 4-aminoantipyrine derivative. *J Mol Struct*, 1320 (2025) 139747.

32 Murail S, De Vries SJ, Rey J, Moroy G & Tufféry P, SeamDock: An interactive and collaborative online docking resource to assist small compound molecular docking. *Front Mol Biosci,* 8 (2021) 716466.

33 Yahaya MAF, Bakar AA, Stanslas J, Nordin N, Zainol M & Mehat MZ, Insights from molecular docking and molecular dynamics on the potential of vitexin as an antagonist candidate against lipopolysaccharide (LPS) for microglial activation in neuroinflammation. *BMC Biotechnol*, 21 (2021) 38.

34 Fu L, Shi S, Yi J, Wang N, He Y, Wu Z, Peng J, Deng Y, Wang W, Wu C, Lyu A, Zeng X, Zhao W, Hou T & Cao D, ADMETlab 3.0: an updated comprehensive online ADMET prediction platform enhanced with broader coverage, improved performance, API functionality and decision support. *Nucleic Acids Res*, 52 (2024) 422431.

35 Ahmad I, Khan H & Serdaroğlu G, Physicochemical properties, drug-likeness, ADMET, DFT studies and in vitro antioxidant activity of oxindole derivatives. *Comp Biol Chem,*104 (2023) 107861.

36 Pirzada AS, Khan H, Alam W, Darwish HW, Elhenawy AA, Kuznetsov A & Daglia M, Physicochemical properties, pharmacokinetic studies, DFT approach, and antioxidant activity of nitro and chloro indolinone derivatives. *Front Chem,* 12 (2024) 1360719.

37 Akhter H, Ritu SS, Siddique S, Chowdhury F, Chowdhury RT, Akhter S & Hakim M, *In silico* molecular docking and ADMET prediction of biogenic zinc oxide nanoparticles: Characterization, and *in vitro* antimicrobial and photocatalytic activity. *RSC Adv*, 14 (2024) 3620936225.

38 Zainab A, Alam A, Khan IA, Elhenawy AA, Shah AJ, Ali M, Ahmad M & Yu H, Polyhydroquinoline amides: comprehensive study on synthesis, *in vivo* biological activities, and computational analysis including molecular docking, DFT, and ADMET. *ACS Omega*, (2025).

39 Sanches IH, Braga RC, Alves VM & Andrade CH, Enhancing hERG risk assessment with interpretable classificatory and regression models. *Chem Res Toxicol*, 37 (2024) 910922.

40 Ghahremanian S, Rashidi MM, Raeisi K & Toghraie D, Molecular dynamics simulation approach for discovering potential inhibitors against SARS-CoV-2: A structural review. *J Mol Liq,* 354 (2022) 118901.

41 Fatmi MQ, Hofer TS, Randolf BR & Rode BM, Exploring structure and dynamics of the diaquotriamminezinc (II) complex by QM/MM MD simulation. *J Phys Chem B*, 12 (2008) 57885794.

42 Morton KS, Elena AM, Armstrong J & O'Malley AJ, Experimental and modeling studies of local and nanoscale para-cresol behavior: a comparison of classical force fields. *J Phys Chem A*, 127 (2023) 33053316.